The March 1993 Superstorm Cyclogenesis: Incipient Phase Synoptic- and Convective-Scale Flow Interaction and Model Performance

MICHAEL J. DICKINSON, LANCE F. BOSART, W. EDWARD BRACKEN, GREGORY J. HAKIM, DAVID M. SCHULTZ,* MARY A. BEDRICK,+ AND KEVIN R. TYLE#

Department of Earth and Atmospheric Sciences, The University at Albany/SUNY, Albany, New Yok

(Manuscript received 14 October 1996, in final form 31 March 1997)

ABSTRACT

The incipient stages of the 12–14 March 1993 ''superstorm'' (SS93) cyclogenesis over the Gulf of Mexico are examined. Noteworthy aspects of SS93 include 1) it is the deepest extratropical cyclone ever observed over the Gulf of Mexico during the 1957–96 period, and 2) existing operational prediction models performed poorly in simulating the incipient cyclogenesis over the northwestern Gulf of Mexico. A dynamic-tropopause (DT) analysis shows that SS93 is triggered by a potent potential vorticity (PV) anomaly as it crosses extreme northern Mexico and approaches the Gulf of Mexico. The low-level environment over the western Gulf of Mexico is warmed, moistened, and destabilized by a persistent southerly flow ahead of the approaching PV anomaly. Ascent and a lowering of the DT (associated with a lowering of the potential temperature) ahead of the PV anomaly contributes to further destabilization that is realized in the form of a massive convective outbreak.

An examination of the National Centers for Environmental Prediction (NCEP) Medium Range Forecast (MRF) model-initialized fields after convection begins shows that the MRF does not fully resolve important features of the potential temperature, pressure, and wind fields on the DT in the incipient SS93 environment. Similarly, the NCEP MRF 12-h/24-h forecasts verifying 1200 UTC 12 March and 0000 UTC 13 March are unable to simulate sufficient deep convection over the Gulf of Mexico, low-level PV growth in the incipient storm environment, high-level PV destruction and the associated warming and lifting of the DT over and downshear of the developing storm. Given that the MRF-initialized fields possess sufficient conditional instability, moisture, and ascent to trigger widespread deep convection, the poorly forecast incipient SS93 development appears to be associated with the failure of the model cumulus parameterization scheme. A comparison of the MRF forecasts with selected forecast fields derived from the European Centre for Medium-Range Weather Forecasts operational model supports this interpretation.

1. Introduction

The winter storm of 12–14 March 1993 (also known as ''the storm of the century'' and ''Superstorm '93,'' hereafter SS93) was a phenomenal meteorological event. Human activity was significantly disrupted over the eastern third of the United Sates. Parts of the Gulf Coast, Florida, and the Caribbean Islands were affected by flooding rains, severe wind damage and associated storm surges, and tornadoes (Kocin et al. 1995; Alfonso and Naranjo 1996). SS93 was responsible for heavy snows (>75 cm) and several low pressure records from the Carolinas to the Canadian Maritimes (Kocin et al. 1995, their Table 1 and Fig. 1). Given the destructive nature of SS93, it has received considerable attention in the literature (see, e.g., Hsu 1993; Gilhousen 1994; Kocin et al. 1995; Uccellini et al. 1995; Caplan 1995; Huo et al. 1995; Orlanski and Sheldon 1995; Alfonso and Naranjo 1996; Bosart et al. 1996; Schultz et al. 1997).

To put the SS93 development into perspective, the National Centers for Environmental Prediction (NCEP, formerly the National Meteorological Center, NMC) twice-daily mean sea level pressure analyses archived on CD-ROM (Mass et al. 1987) were searched for all occurrences of local pressure extrema below 1000 hPa at grid points (NCEP octagonal grid) situated over the Gulf of Mexico and immediate coastal regions for November–April of 1957–1989. The number of individual cyclones associated with these occurrences, stratified by gridpoint central pressure, is shown in Table 1. The results attest to the rarity of cool season cyclones with a central pressure less than 1000 hPa over the Gulf of Mexico. The lowest gridded central pressure (988.7 hPa)

* Current affiliation: NOAA/National Severe Storms Laboratory, Norman, Oklahoma.

+ Current affiliation: Aeromet, Inc., Kwajalein Atoll, Marshall Islands.

Current affiliation: General Sciences Corporation, Laurel, Maryland.

Corresponding author address: Michael J. Dickinson, Department of Earth and Atmospheric Sciences, The University at Albany/SUNY, 1400 Washington St., Albany, NY 12222.
E-mail: mjd@atmos.albany.edu

TABLE 1. Climatology of sea level pressures in the cold season (November–April) 1957–89. Number of occurrences of sea level pressure minima less than or equal to 1000 hPa in the Gulf of Mexico in the cold season (November–April) from 1957 to 1988. The asterisk represents the cyclone of 17–18 March 1983 (987-hPa minimum from the NMC gridded data, but with a minimum pressure from the NMC surface analysis at 1200 and 1500 UTC 17 March of 982 hPa).

Depth of central sea level pressure	Number of occurrences
$p < 990$ hPa	1*
$p \leq 992$ hPa	5
$992 < p \leq 996$ hPa	21
$996 < p \leq 1000$ hPa	180

occurred with the 17–18 March 1983 cyclone. The NCEP 3-h manual analyses available on 35-mm microfilm revealed a 982-hPa central pressure at 1200 UTC 17 March 1983 when this cyclone was situated over the northeast Gulf of Mexico. This value should be compared with the 975-hPa cyclone central pressure for SS93 prior to landfall over northwest Florida analyzed by Kocin et al. (1995; their Fig. 9). A further manual check of locally archived sea level pressure maps and the Daily Weather Map Series for November 1989 to April 1996 also failed to disclose the existence of any comparably deep cool season cyclones over the Gulf of Mexico, leading us to conclude that SS93 was the deepest cool season storm to affect the Gulf of Mexico during the 1957–96 period.

To help motivate our study of SS93's extraordinary strength in the Gulf of Mexico, we present in Fig. 1a the surface central pressure versus latitude for four memorable eastern North American storms that have been studied extensively in the literature. Although the storms of March 1971 (Carr and Kennedy 1982; Boyle and Bosart 1986), January 1978 (Burrows et al. 1979; Salmon and Smith 1980; Hakim et al. 1995, 1996), and March 1984 (Gyakum and Barker 1988; Kuo et al. 1995; Gyakum et al. 1995) all achieved a comparable or lower central pressure than SS93, none of them were as deep as SS93 at low latitudes.

The unusually robust early intensification of SS93 (Fig. 1a) was not well simulated by the NCEP operational Regional Analysis and Forecast System (RAFS) and Medium Range Forecast Model (MRF). This error is apparent from Fig. 1b, which shows the forecasted central pressure of SS93 versus latitude for the RAFS–MRF forecasts initialized 0000 and 1200 UTC 12 March. Comparison with analyses given by Kocin et al. (1995) (identified as ''observed'' in Fig. 1b) shows that the RAFS–MRF forecasts underestimated the cyclone central pressure by approximately 20 hPa during the 24-h development period ending 1200 UTC 13 March. These large forecast underestimates of cyclone central pressure occurred during a period of widespread intense convection near the storm center (discussed in section 3b). These pressure errors during the initial cyclogenesis stand in sharp contrast to the excellent MRF forecasts [as well as other operational model forecasts, e.g., Caplan (1995)] during the later stages of the storm's life cycle (Fig. 1b). Despite these shortcomings, however, the MRF model performed admirably in alerting forecasters several days in advance that a cyclone of historic proportions was likely. Readers interested in a detailed assessment of NCEP model performance during SS93 should consult Caplan (1995) and Uccellini et al. (1995). They should consult Huo et al. (1995) to see how a mesoscale research version of the Canadian Regional Finite Element (RFE) model simulated SS93.

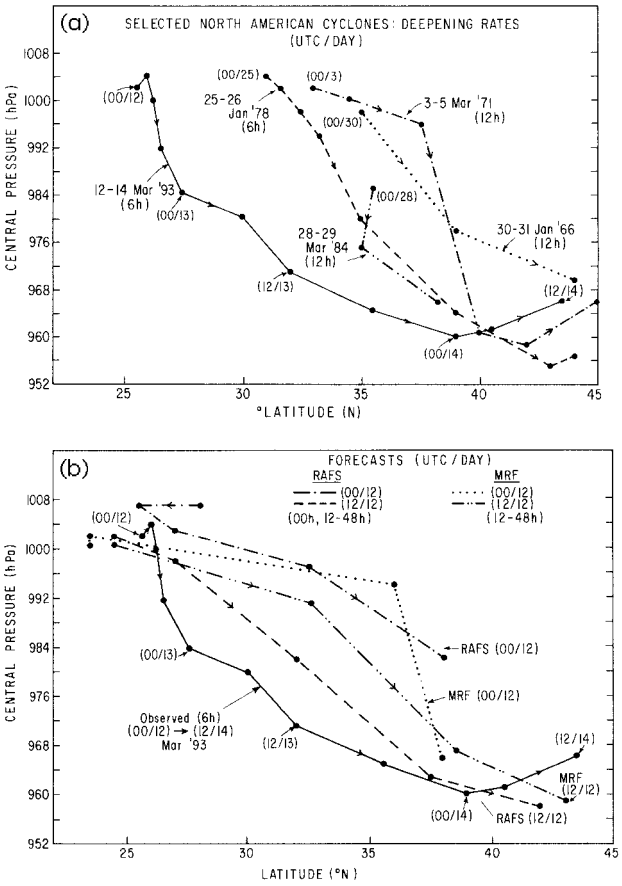

FIG. 1. (a) Sea level pressure (hPa) versus latitude for five selected North American cyclones, including SS93. Time interval is 12 h except 6 h for SS93 and the 25–26 January 1978 cyclone. (b) As in (a) except for selected MRF and RAFS SS93 forecasts. Observed central pressure values taken from Kocin et al. (1995) surface analyses.

The purpose of this paper is to document the exceptional initial intensity of SS93 and to explore the possible physical mechanisms responsible for the explosive incipient cyclogenesis. Given that widespread deep convection accompanied the initial SS93 development, and given that the NCEP model forecasts significantly underestimated the storm intensity during this phase of development, we hypothesize that the model's inability to simulate properly the bulk effects of cumulus convection contributed significantly to the poor forecasts. We employ a potential vorticity (PV) perspective based

on the concept of a dynamical tropopause (DT) (Hoskins et al. 1985; Hoskins 1990) to facilitate our analysis. The PV viewpoint has been used by a number of authors (e.g., Hoskins and Berrisford 1988; Davis 1992a,b; Bosart and Lackmann 1995; Bosart et al. 1996; Davis et al. 1996; Hakim et al. 1995, 1996) to diagnose a spectrum of cyclogenesis events. This paper is organized as follows: section 2 describes the data and methodology, section 3 provides an overview of the initial cyclogenesis, section 4 discusses the model representation of the initial cyclogenesis, and the concluding discussion and perspective appears in section 5.

2. Data and methodology

To describe the evolution of the storm and to help identify the forecast errors, we employ MRF model 0–48-h forecasts from 0000 UTC 12 March to 0000 UTC 14 March obtained from the National Center for Atmospheric Research (NCAR) on an equivalent resolution of 2.5° × 2.5° (the operational MRF forecasts were generated at T126 resolution). The dataset consists of geopotential heights, temperatures, and winds on 12 vertical levels extending from 1000 hPa to 100 hPa every 12 h. This dataset was supplemented with the 2.5° × 2.5° MRF final analyses and MRF forecast accumulated and convective precipitation grids, interpolated to a 1° × 1° grid. European Centre for Medium-Range Weather Forecasts (ECMWF) uninitialized gridded analyses on 13 vertical levels extending from 1000 hPa to 50 hPa were also obtained from NCAR to compare against the MRF fields. The ECMWF 2.5° × 2.5° grids were obtained by decomposing the archived spectral coefficients stored at NCAR. NCEP sea surface temperature (SST) values were obtained from NCAR on a 2.5° × 2.5° grid. The MRF, ECMWF, and SST gridded analyses were stored, analyzed, and displayed using the Generalized Meteorological Analysis Package (GEMPAK, Koch et al. 1983).

We also employed conventional surface and upper-air observations, including Mexican and Central American hourly observations, to help document the incipient SS93 cyclogenesis. Lightning data was provided by the National Lightning Detection Network (NLDN). Hard copy visible and infrared (IR) satellite imagery was available from the University at Albany/SUNY archives and in digital form from Space Science and Engineering Center (SSEC) at the University of Wisconsin in Madison, Wisconsin.

Ertel PV is calculated on isobaric surfaces using

$$q = -g\frac{\partial\theta}{\partial p}\left(f + \frac{\partial v}{\partial x} - \frac{\partial u}{\partial y}\right) + g\left(\frac{\partial v}{\partial p}\frac{\partial\theta}{\partial x} - \frac{\partial u}{\partial p}\frac{\partial\theta}{\partial y}\right) \quad (1)$$

where q represents Ertel PV, θ represents the potential temperature, u and v represent the zonal and meridional components of the wind, respectively, g is gravity, f is the Coriolis parameter, and the other terms have their usual meteorological meaning. The DT (e.g., Hoskins and Berrisford 1988; McIntyre 1988) is determined from the orientation of the 1.5 PV unit (PVU) surface and values of u, v, θ, p are interpolated to the 1.5-PVU surface (1 PVU = 10^{-6} K m^2 kg^{-1} s^{-1}) from above (θ_T and p_T will refer to the values of θ and p on the DT, respectively).[1]

3. Overview of initial cyclogenesis

The track of SS93 and the important PV anomalies (Bosart et al. 1996) are shown in Fig 2a and are further discussed in section 3a. We will use the shorthand notation (UTC/day) to denote times and dates. The track of SS93, at 6-h intervals, and the NCEP SST analysis averaged from 00/11 to 00/13 are shown in Fig. 2b. Note that because of the coarse resolution of the SST analysis, the warm ocean eddies and the strong coastal SST gradient shown by Gilhousen (1994, his Fig. 10) are not readily apparent in Fig. 2b (see also section 6d).

a. Synoptic-scale dynamical tropopause representation

Hoskins et al. (1985), Davis and Emanuel (1991), Raymond (1992), and Hakim et al. (1995, their section 4), among others, have outlined the benefits of using the DT approach in identifying upper-tropospheric disturbances associated with cyclogenesis. This method was also utilized by Bosart et al. (1996) in their analysis of the antecedent conditions associated with SS93 and is adopted here. Strong jet streams are marked by large gradients of potential temperature θ_T and pressure p_T. Likewise, the conservation property of θ_T on the DT for adiabatic and inviscid flows allows for the tracking of precursor PV disturbances on the DT and also facilitates the identification of regions where significant nonconservative processes (e.g., latent heat release) are present. Typically, the DT is ''lifted'' due to decreasing upper-level PV above a region of widespread condensation.

Maps of θ_T, p_T, winds, and vertical velocities on the DT were derived from the initialized and model forecast fields at all times. Figure 3 shows θ_T, θ_T advection, and winds (top) and p_T and vertical motion (bottom) at 12-h intervals for the 24-h period ending 00/13 for the MRF initialized fields. As discussed by Bosart et al. (1996), two PV anomalies are present in the STJ prior to the period of incipient cyclogenesis (C and D in Fig. 3 of Bosart et al. 1996 and Fig. 2a here) and cross the west coast of the United States subsequent to 12/10. The leading, and weaker, of the two PV anomalies, D, moves onshore over California and then turns southeastward

[1] Due to diabatic effects, PV values in the lower troposphere occasionally may exceed 1.5 PVU. Thus, interpolation upward from the surface may intercept these low-level positive PV anomalies resulting in an artificially low tropopause height.

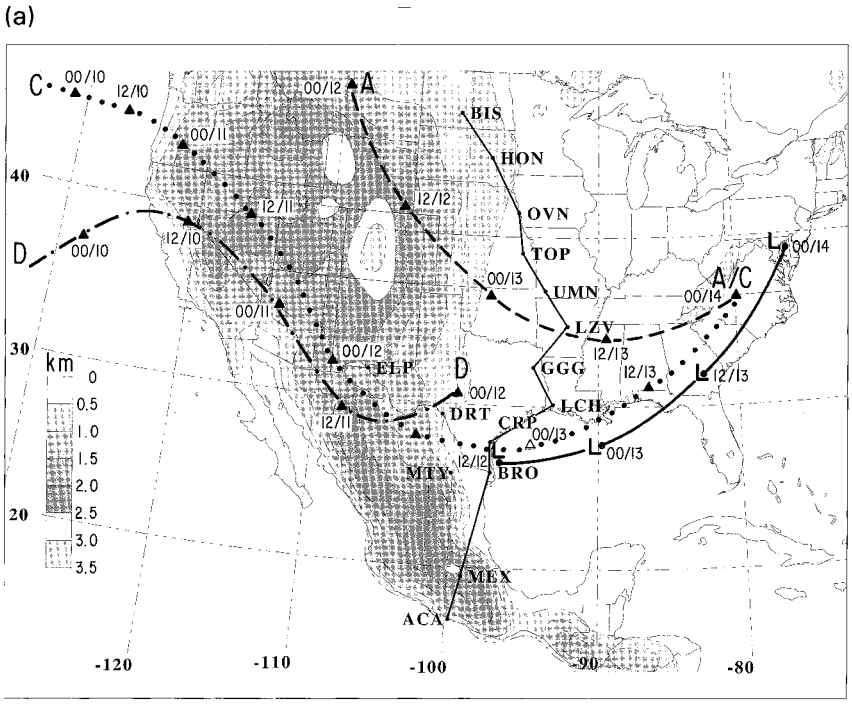

FIG. 2a. Map illustrating simplified terrain (km, shaded according to scale at left) and sounding stations (three-letter identifiers) mentioned in the text. Cross section shown in Fig. 13 is marked by a thin solid line. Tracks and 12-h positions (UTC/day; March 1993) of PV anomalies A, C, and D are indicated by the dashed, dotted, and long dash–dotted lines, respectively. Solid line denotes track of SS93; "L" symbol marks the cyclone position every 12 h.

toward Texas where it dissipates by 00/12 (Fig. 2a). Trailing PV anomaly C moves onshore over Oregon by 00/11 and by 00/12 is located near the southern border of New Mexico (Fig. 2a).

As discussed by Bosart et al. (1996), cyclogenesis is triggered over the southern Texas coastal waters prior to 12/12 as PV anomaly C crosses extreme northern Mexico. This interpretation is made more explicit in Fig. 3a. The advection of lower values of θ_T over the northwestern Gulf of Mexico subsequent to 00/12 heralds the approach of PV anomaly C. This θ_T advection pattern leads to an increase in the difference between θ_T and θ_e (equivalent potential temperature) at 850 hPa, referred to as the coupling potential (hereafter CP). Negative values of the CP indicate the atmosphere is susceptible to deep convection, given a suitable lifting mechanism and adequate moisture. Note also that by 12/12 the area of ascent on the DT marking PV anomaly C has come into juxtaposition with an area favorable for deep convection characterized by negative CP values (cf. Figs. 3a,b and 14d,e). Explosive cyclogenesis ensues as PV anomaly A, initially situated over Montana at 00/12 (Fig. 3a), moves southeastward and begins to interact with PV anomaly C by 00/13 (Fig. 3c). This interaction is manifest by the drawing together of the twin ribbons of strong θ_T gradients marking the polar front jet (PFJ) and STJ after 12/12. The strengthening of the θ_T gradient from Arkansas northeastward to the lower Great Lakes by 00/13 occurs in response to a significant increase in θ_T over the southeastern United States. Note also the steadily increasing gradient of p_T downstream of PV anomalies A and C (Fig. 3f) that marks the axis of the strengthening southwesterly PFJ over the Great Lakes region in which wind speeds exceed 75 m s^{-1} by 12/13 (Fig. 3c).

A DT analysis comparable to that shown in Fig. 3, but based upon the MRF 2.5° *uninitialized* fields, provides a check on the quality of the MRF initialization. The results (not shown) differ little from Fig. 3. As a check on the impact of model analysis we display in Fig. 4 a comparable DT analysis to Fig. 3 based upon the ECMWF 2.5° × 2.5° uninitialized fields. Note that our objective is not to provide an explicit detailed comparison of the MRF and ECMWF models but rather to show that the MRF captures the salient features of SS93. Although the broad patterns in Figs. 3 and 4 are similar (e.g., the signatures of PV anomalies A and C and the poleward displacement of the θ_T contours across the flow in the developing ridge over eastern North America in the 12 h ending 00/13), the gradients of p_T and θ_T are sharper and better defined in the ECMWF analyses. An important difference between Figs. 3 and 4, however, is that the ECMWF analysis shows much more southerly flow over the northwest Gulf of Mexico and the Texas coast ahead of PV anomaly C at 12/12. The ECMWF analysis appears to replicate the observed southerly flow

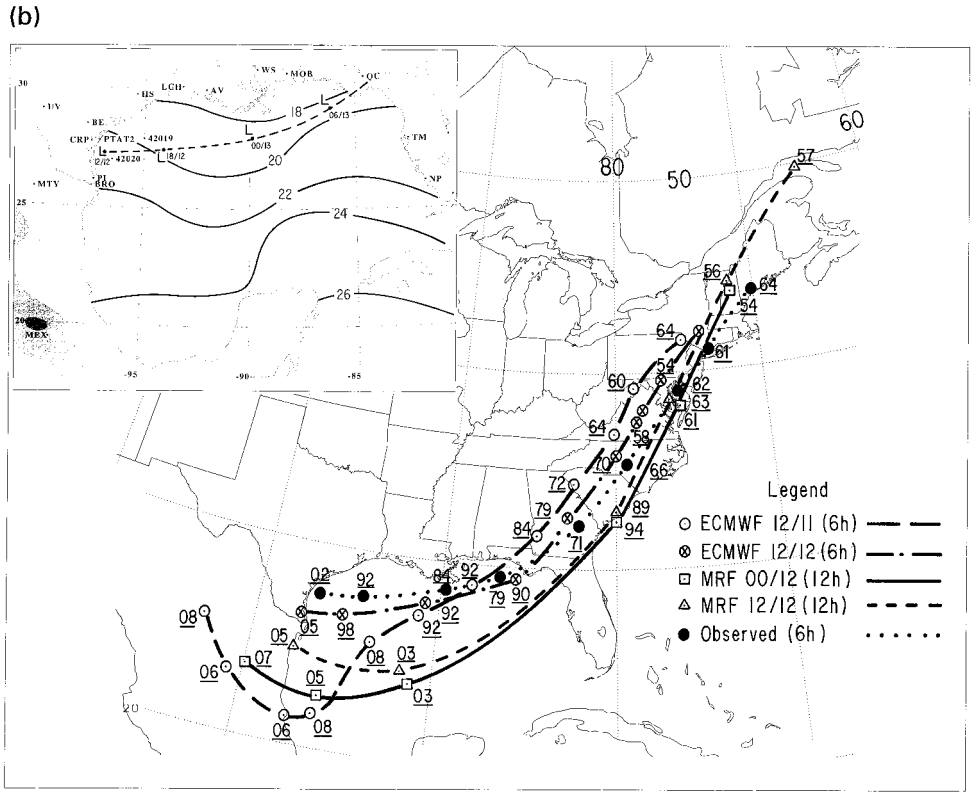

FIG. 2b. Upper-left corner: location map for selected surface and upper-air stations (three-letter identifications) and National Lightning Detection Network station locations (two-letter identifications). Sea surface temperatures (solid, every 2°C) from the NCEP global analyses. Track of SS93 is shown by the dashed line with times (UTC/day; March 1993) indicated every 6 h. Main figure: MRF and ECMWF forecast storm tracks and observed storm track for model time shown in the legend. Cyclone positions shown every 6 h (except every 12 h for the MRF). Central pressure (leading 9 or 10 omitted) shown in hectopascals.

in the 400–200-hPa layer in this region (discussed more fully in section 3b) better than the MRF. Clearly, however, the MRF analysis represents adequately the large-scale circulation features associated with the SS93 cyclogenesis.

The impact of the convection on the DT structure is shown in Fig. 3. At 00/12, the 325-K isentrope is oriented west–east across extreme northern Mexico and southeastern Texas and then extends northeastward along the Texas Gulf Coast (Fig. 3a). By 12/12 (Fig. 3b), the θ_T = 320 and 325 K isentropes have shifted slightly northwestward and are now oriented southwest–northeast from central Texas to central Mississippi. The observed poleward bulge of these isentropes from coastal southeastern Texas to Alabama occurs as winds on the DT slowly back through 12/12 and cannot be explained by quasi-horizontal advective processes acting alone. The θ_T increase must then be associated with nonconservative processes, more specifically, the release of latent heat associated with deep convection. Associated with the poleward bulge of the θ_T = 320 and 325 K isentropes (Figs. 3a,b) is the development of an area of $p_T < 250$ hPa centered over Louisiana and Mississippi as the DT is uplifted downstream of the convection near BRO and CRP (Figs. 3d,e).

Nonconservation of θ_T is especially prominent between 12/12 and 00/13, as shown by the increased elevation of the DT (higher θ_T and lower p_T, Figs. 3c,f) across the southeastern portion of the United States as typified by the closed θ_T = 365 K contour at 00/13. Associated with the large increase in θ_T is a pronounced decrease in p_T as the DT is uplifted downstream of the rapidly intensifying storm and associated deep convection. This p_T decrease is realized by a large poleward shift of the 200-hPa contour across Tennessee and the southern Ohio Valley by 00/13 (cf. Figs. 3e,f) as the DT rises. Additional comparison of Figs. 3b,c,e,f and 4b,c,e,f reveals that the ECMWF DT analyses capture the well-known ''PV hook'' that is a signature of explosive cyclogenesis (see, e.g., Davis et al. 1996; Hakim et al. 1995, 1996) by 00/13. The ''PV hook'' is created by differential advection of θ_T and p_T (not shown) in the region of strong westerly flow pushing eastward across the Gulf of Mexico ahead of PV anomaly C.

The θ_T and p_T advection patterns also illustrate the ''compaction'' of PV anomaly C, defined as an increase

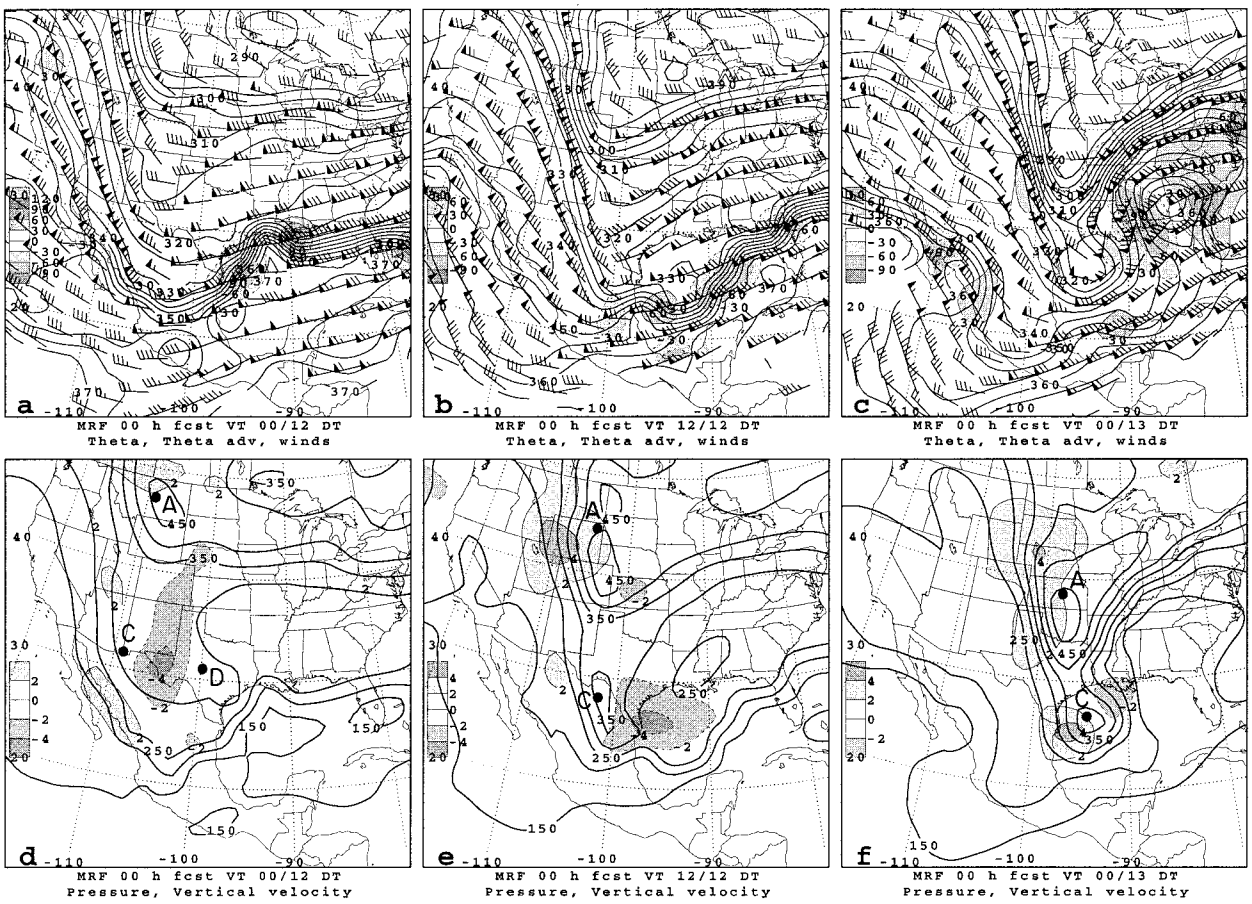

FIG. 3. MRF-initialized dynamic tropopause maps based on the 1.5 potential vorticity unit (PVU) surface (1.0 PVU = 10^{-6} m^2 s^{-1} K kg^{-1}). Panels (a), (b), and (c) show the winds (one pennant, full barb, and half-barb denote 25, 5, and 2.5 m s^{-1}, respectively), θ_T (solid, every 5 K), and θ_T advection [K (12 h)$^{-1}$, shaded every 30 K (12 h)$^{-1}$] by the scale at the left at (UTC/day; March 1993) 00/12, 12/12, and 00/13, respectively. Panels (d), (e), and (f) show p_T (solid, every 50 hPa) and vertical velocity (shaded, every 2 hPa s^{-1}, scale at left) at (UTC/day; March 1993) 00/12, 12/12, and 00/13, respectively. Positions of PV anomalies A, C, and D (Fig. 2a) are shown on panels (d), (e), and (f) for reference.

in the gradient of θ_T and p_T along the flow direction, beginning 12/12 and more significantly by 00/13. The compaction of PV anomaly C is also seen as a shortening of the distance between the p_T trough and the downstream p_T ridge that is forming downshear of the convection at 12/12 (Figs. 3d,e). The PV anomaly compaction can be an important precursor signal for cyclogenesis (Lackmann et al. 1997), given that height falls and ascending motion can be associated with positive PV advection (Hoskins et al. 1985). (The isobaric equivalent of PV anomaly compaction is increasing cyclonic vorticity advection in association with increasing flow curvature.) The compaction of PV anomaly C associated with deep convection over the Gulf of Mexico and its interaction with PV anomaly A, well under way by 00/13 (Fig. 3c), culminates in the spectacular cyclogenesis known as SS93 over the following 36-h period (see, e.g., Kocin et al. 1995; Huo et al. 1995; Bosart et al. 1996; Bosart 1997). The compaction process can also be related to the self-development concept of Sutcliffe and Forsdyke (1950) and Petterssen (1955). Deepening cyclones associated with convection near the center (Tracton 1973) and the reintensification of a tropical storm over land (e.g., Bosart and Lackmann 1995) are examples of self development in which positive PV advection is increased near the center.

b. Observational overview

1) SURFACE θ_e EVOLUTION

Surface observations show a band of high-θ_e (>335 K) air extending northwestward from the Gulf of Mexico into southern Texas along the Rio Grande Valley at 00/12 (Fig. 5a). These high θ_e values are a reflection of anomalously warm SSTs in the Gulf of Mexico and the poleward surge of warm moist air ahead of PV anomaly C at this time (Fig. 2b and Gilhousen 1994, his Fig. 10). A strong θ_e gradient runs east–west along the northern Gulf Coast and extends into central Texas (Fig. 5a).

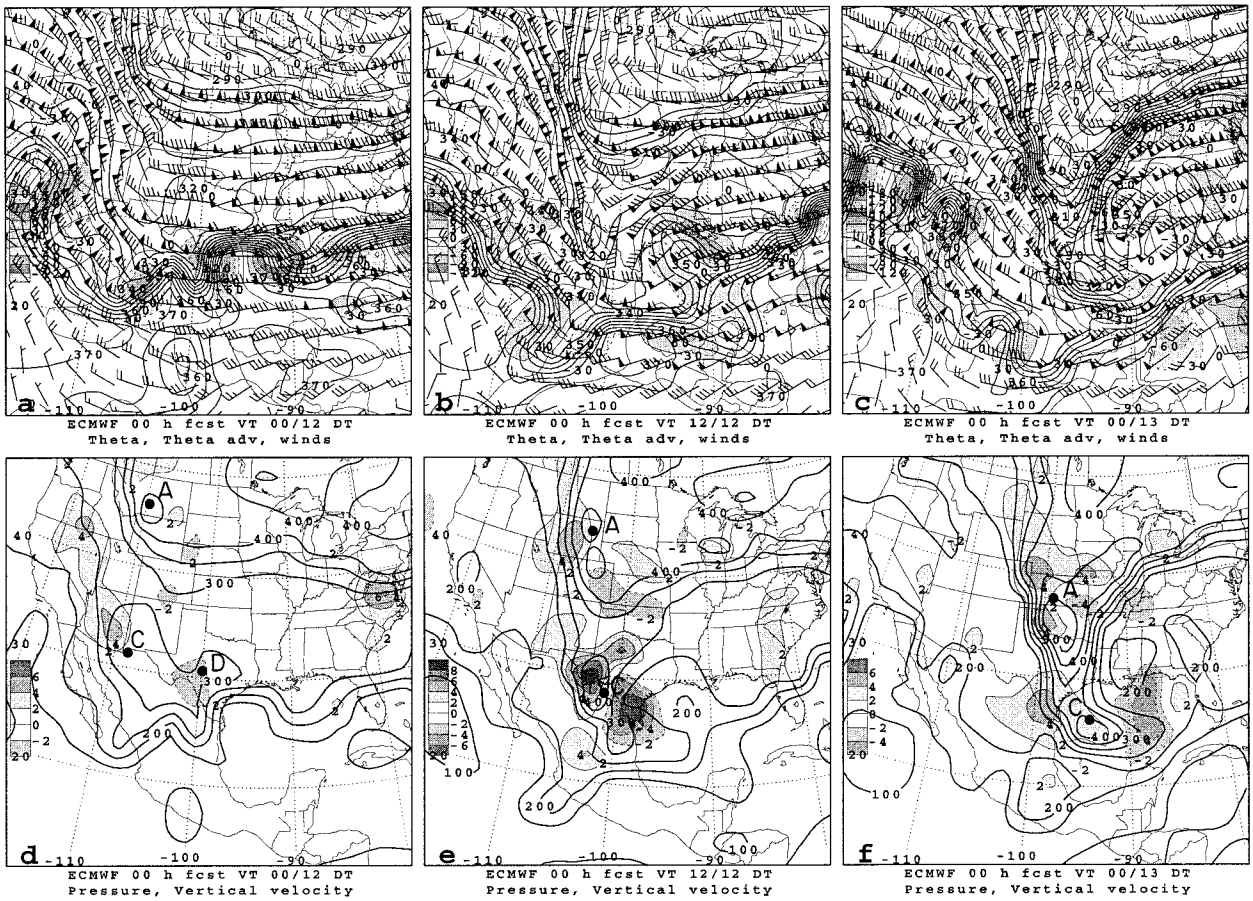

FIG. 4. As in Fig. 3 except for ECMWF uninitialized fields.

For brevity, this θ_e gradient will be referred to as the coastal baroclinic zone (CBZ). Southerly flow across the western Gulf of Mexico provides a source of moisture to interior Texas. Maximum potential instability, as measured by a relative maximum in convective available potential energy (CAPE), is associated with the high-θ_e band over southeastern Texas at 00/12 (Figs. 5a, 14d). Note also that the high-θ_e band shown in Fig. 5a and the area of highest (lowest) CAPE (CP) values seen in Fig. 14d are nearly colocated.

2) SATELLITE, LIGHTNING, AND PRECIPITATION OVERVIEW

Infrared satellite imagery (Fig. 6) and cloud-to-ground (CG) lightning maps (Fig. 7) are shown for the period from 03/12 to 12/13. High, cold cloud tops are present in northeast Texas, associated with the remnant convection of dissipating PV anomaly D at 03/12 (Fig. 6a). The rapid growth of relatively cold cloud tops after 06/12 signifies the onset of widespread deep convection across southern Texas (Figs. 6b,c), with very intense convection indicated by 12/12 (Fig. 6d). By 00/13 a squall line (Fig. 6e) expands equatorward to the Yucatan Peninsula (Fig. 6f) and is especially well organized as it crosses Florida and Cuba from 0600 to 1200 UTC 13 March (Figs. 6g,h).

Evidence for significant convection over the Gulf of Mexico is seen in the ship and buoy reports. DeAngelis et al. (1993) present a barogram trace from the oceanic vessel *Inger* (their figure is unnumbered) while it was in the Gulf of Mexico on route to New Orleans, Louisiana. The *Inger* encountered the squall line shortly after 22/12 (estimated ship position is 25.6°N, 87.2°W) when the pressure fell abruptly from 1000 to 994 hPa in less than 40 min and then rose equally rapidly back to an ambient 1000 hPa in the trailing bubble high. Beginning around 0030 UTC 13 March the pressure fell about 4 hPa in less than 20 min, then fell more slowly for approximately 1 h, and then fell more rapidly again, culminating in a sharp V-shaped pressure minimum near 990 hPa shortly after 03/13. The *Inger* pressure trace is remarkably similar to pressure traces seen at continental locations that have experienced a vigorous squall line passage ahead of a sharp cold front. Note also that the *Inger* pressure observations agree very well with the vigorous squall line depicted in the satellite-derived rainfall rate estimates for 0245 UTC 13 March shown

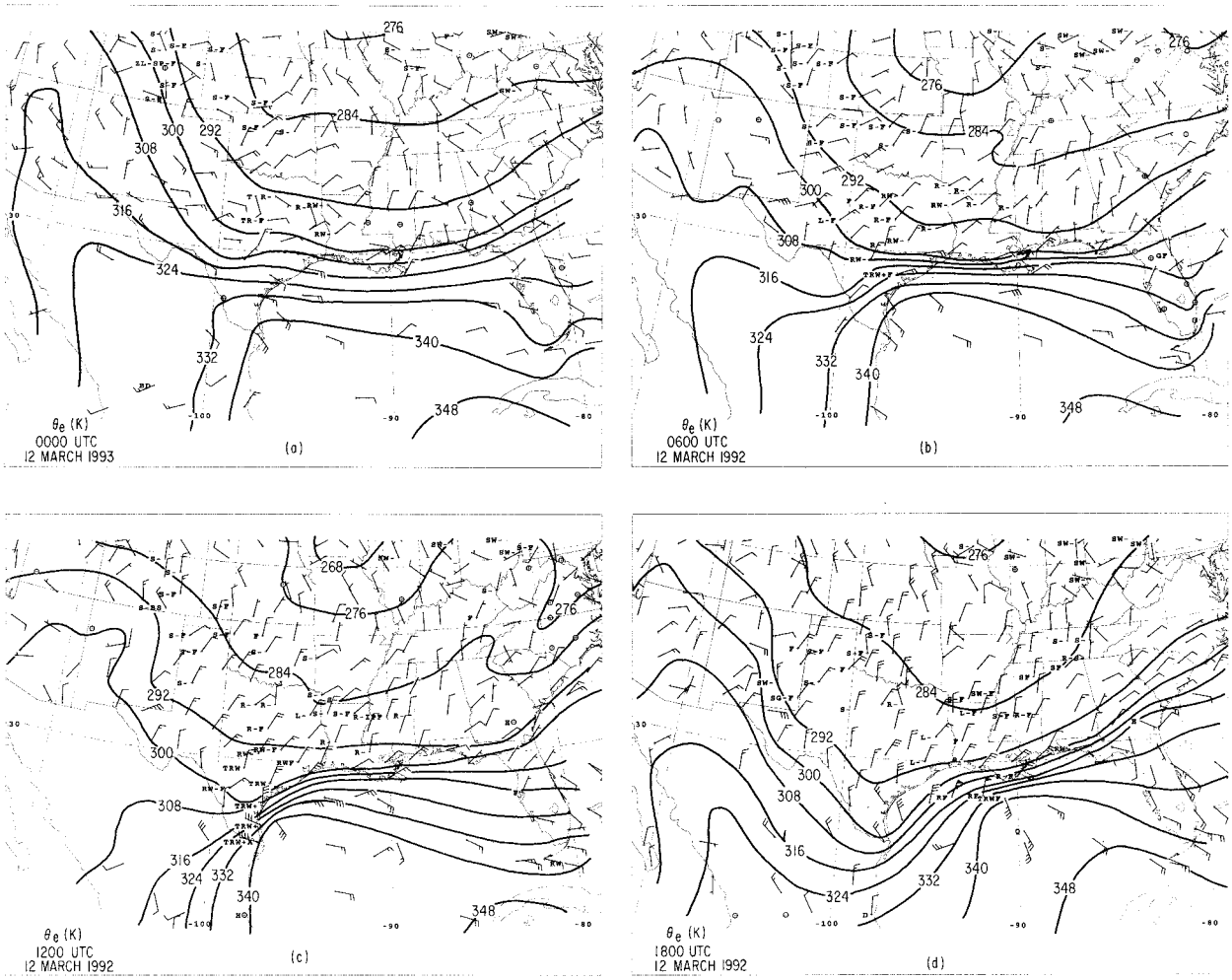

FIG. 5. Observed current surface weather (conventional plotting), equivalent potential temperature (solid lines, every 8 K), and winds (see Fig. 3) at (UTC/day; March 1993) (a) 00/12, (b) 06/12, (c) 12/12 and (d) 18/12, respectively.

in Fig. 8 and the CG lightning plot for the 6-h period ending 00/13 (Fig. 7f). Additional confirmation comes from the barogram trace from the oceanic ship *Columbia Bay* presented in Walker (1993). This pressure trace, similar to the *Inger's*, shows an initial 5-hPa pressure plunge and trailing bubble high recovery between 18/12 and 19/12 (estimated ship position is 26.7°N, 90.4°W) and then a further fall to a V-shaped pressure minimum (~990 hPa) near 21/12.

The CG-lightning activity provides further evidence of the growth of deep convection across southern Texas in the incipient SS93 environment. CG lightning flash activity in east-central Texas north of the CBZ gradually diminishes in frequency and aerial coverage through 09/12 as PV anomaly D dissipates (Figs. 6c,d and 7b,c). Meanwhile, sporadic convection in southern Texas near the southwestern end of the CBZ by 03/12 (Fig. 7a) becomes increasingly better organized and more widespread through 12/12 (Figs. 7b,c,d) with the approach of PV anomaly C toward the Gulf of Mexico.

Figure 9 shows the 12-h accumulated precipitation at 12-h intervals from 12/12 to 12/13. Two distinct precipitation maxima are present across Texas at 12/12. The first, associated with the convection initiated by PV anomaly D, is located across northeastern Texas extending into northern Louisiana. The second is located across southern Texas (Fig. 9a) associated with the explosive convective outbreak triggered by the approach of PV anomaly C. Twelve hours later (Fig. 9b) the maximum precipitation is confined to coastal Louisiana on the northern edge of the high cloud shield (Fig. 6e) and CG-lightning activity (Fig. 7e). By 12/13 the maximum precipitation is aligned along two distinct bands (Fig. 9c). The first band extends northeastward from the Florida panhandle along the Appalachians into North Carolina immediately to the left of the track of SS93 (Figs. 2, 6h). The second band is associated with relatively cold cloud tops (Figs. 6g,h) and numerous CG lightning flashes (Figs. 7g,h) and is oriented west–east across central Florida in conjunction with the powerful squall line

crossing the region. Maximum precipitation rates along this squall line exceed 40 mm h^{-1} across the Gulf of Mexico, providing further evidence of the intensity of the deep convection (Fig. 8). Precipitation rates across the Florida panhandle and extending into Mississippi, Alabama, and Georgia average in the 10–20 mm h^{-1} range (Fig. 8).

3) VERTICAL STRUCTURE

A sounding analysis is introduced to help link the synoptic- and convective-scale interactions in the incipient SS93 environment. The apparent dissipation of PV anomaly D in the MRF analysis over northeast Texas after 00/12 (Figs. 6a and 7a,b) is associated with an area of weak convection on the northern side of the CBZ (Figs. 5a, 6a, and 7a). The 00/12 Longview (GGG), Texas, sounding (nominal sounding launch at 2315 UTC) presented in Fig. 10a shows evidence of a warm frontal inversion near 850 hPa, a stable layer from 850 to 700 hPa and a near-moist-adiabatic layer from roughly 600 to 300 hPa. The convection in the vicinity of GGG (Figs. 7a, 10a) exhibits the characteristics shown by Colman (1990a,b) for thunderstorms that develop above the planetary boundary layer (PBL) in regions of high baroclinicity with strong vertical wind shear, low-level warm advection, a deep near-moist-adiabatic layer above and little, if any, positive CAPE. The dissipation of PV anomaly D ensures a continued moist southeasterly flow across southern Texas. As noted by Bosart et al. (1996), the associated relatively low sea level pressures and absence of cyclogenesis over Texas precludes strong pressure rises and an associated equatorward surge of cold air east of the Rockies.

The 12/12 sounding at Monterrey (MTY), Mexico (Fig. 10b), indicates the vigor of the rapidly developing storms at the southwestern edge of the convective area. Above the PBL the temperature profile is nearly moist adiabatic up to 350 hPa with the exception of the 775–575-hPa layer. A small inversion near 350 hPa collocated with an approximately 50-hPa-thick layer of easterly flow may signify the convective outflow in rapidly expanding anvils. Although it is not possible to verify this speculation, given the coarseness of the sounding network and the absence of detailed observations, the location of MTY along the extreme southwestern edge of the rapidly expanding satellite-observed high-cloud shield (Figs. 6b,c,d) suggests that the radiosonde balloon probably entered the growing anvil near 350 hPa (note the approximate saturation with respect to ice above the inversion) where it encountered a layer of easterly flow. The vigor of the convection along the southwestern flank of the storm region and the general east-southeastward movement of the convection are symptoms of the deepening large-scale trough and resulting merger of PV anomalies A and C.

Figures 11a,b show the 00/12 observed soundings for El Paso (ELP) and Del Rio (DRT), Texas—the two stations located closest to the PV anomaly C (Fig. 3a). For comparison, the ECMWF-uninitialized and MRF-initialized soundings interpolated to the location of these two stations are superimposed on the ELP/DRT soundings. The comparison reveals: 1) the ECMWF and MRF initializations represent the observed thermal stratification reasonably well, including the tropopause, with the exception of the observed low-level cooling behind the cold front at DRT, and 2) the MRF initialization captures the observed tropospheric wind profile reasonably well. Furthermore, the MRF initialization is unable to represent properly some of the observed smaller-scale moisture structure (not shown). These observations suggest that the 2.5° MRF initialization captures the essential structure of PV anomaly C at 00/12, including the pocket of cold air in the upper troposphere (300-hPa temperature at DRT is approximately −47°C). This cold-air pocket, when superposed above a warming and moistening PBL, will support deep convection as the ascent ahead of PV anomaly C approaches the Gulf of Mexico.

Figures 12a,b,c show observed, ECMWF, and 0-h and 12-h MRF soundings for Brownsville (BRO) and Corpus Christi (CRP), Texas, and Lake Charles (LCH), Louisiana, at 12/12. Although the models have some difficulty resolving the thermal structure near the ground and at the tropopause, the ECMWF initialization compares more favorably to the observed temperature structure than does the MRF initialization. Also, the MRF-initialized and 12-h forecast wind soundings compare more favorably with each other than to the observed or the ECMWF-initialized soundings (Fig. 12). Specifically, neither the MRF initialization nor the 12-h forecast is able to depict the intensity of the observed low-level southeasterly flow along the Texas and Louisiana coast, the strong southerly flow observed in the 500–200-hPa layer at CRP, the shallow surface-based cold layer and associated warm-air advection at BRO and CRP, the midlevel warmth and southeasterly flow at CRP, and the sharpness (and associated elevated height) of the observed tropopause at all three stations. The sharp tropopause structure is a signature of lapse-rate modification by deep convection and is very analogous to a similar convectively modified sounding for LCH presented by Bosart and Nielsen (1993). The mid- and upper-level southerly (west-northwesterly) flow at CRP (BRO) at 12/12 is a manifestation of the highly diffluent upper-tropospheric flow discussed earlier (recall Figs. 3b and 4b). Given that satellite and lightning data (Figs. 6b,c and 7b,c,d) indicate that organized convection develops rapidly over southern Texas after 06/12, it is likely that the diffluence and the associated PV anomaly C are significantly influenced by convection at 12/12. Note that the MRF initialization and 12-h forecast, both valid for 12/12, fail to represent accurately the thermal and wind structure of the larger-scale environment westward and poleward of the convection.

By 12/12 a surface cyclone with a central pressure of

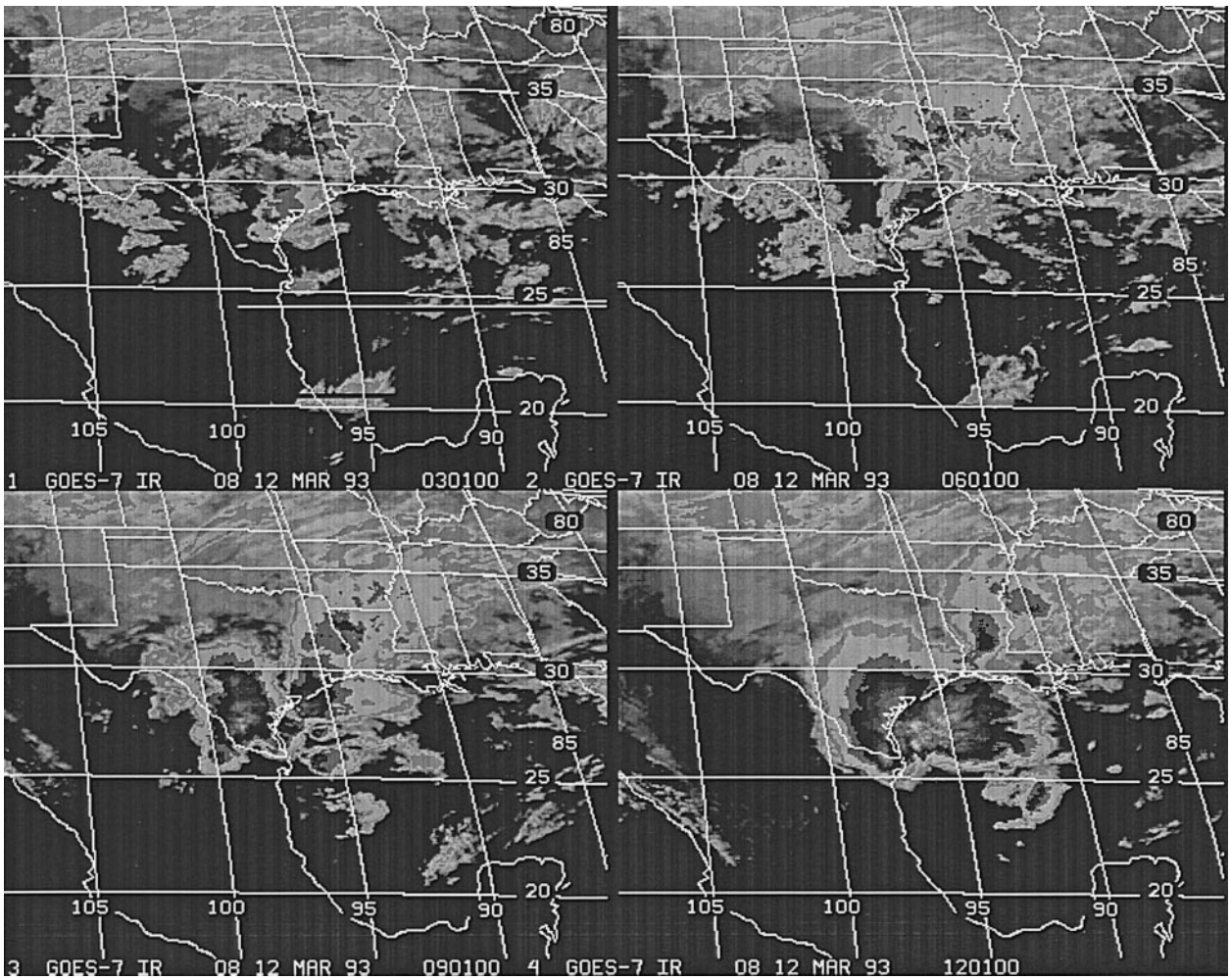

FIG. 6. *GOES-7* infrared satellite imagery shaded according to the operational MB curve (Clark 1983): (a) 0301 UTC 12 March, (b) 0601 UTC 12 March, (c) 0901 UTC 12 March, (d) 1201 UTC 12 March, (e) 1801 UTC 12 March, (f) 0001 UTC 13 March, (g) 0601 UTC 13 March, and (h) 1201 UTC 13 March (all of 1993).

1002 hPa has developed to the east of BRO and is centered over a warm SST anomaly (Figs. 2 and 10 of Gilhousen 1994) beneath this convection. The 12/12 sounding (nominal sounding launch at 1115 UTC) at BRO (Fig. 12a) shows the unstable atmosphere (CAPE of 1604 J kg^{-1} and lifted index of -7°C) ahead of PV anomaly C and immediately ahead of the wind shift associated with the approaching convective line. A deep moist layer extending up to 700 hPa is present at this time. Deep warm-air advection is also present, implying a mechanism for the strong ascent shown in Fig. 3b. By 12/12 the surface winds at BRO have shifted to 270° at 19 m s^{-1} as the leading edge of the convective outflow and associated cold surge triggered by PV anomaly C reaches the Gulf of Mexico (Schultz et al. 1997; their Figs. 2d, 11a).

Given the evidence for widespread deep convection at 12/12, an important issue is whether the MRF misrepresentation of the environmental flow structure in the upper troposphere adversely affects the signature of PV anomaly C. A comparison of the ECMWF-uninitialized and MRF-initialized DT analyses discussed previously (Figs. 3 and 4) indicates that the overall signature of PV anomaly C is represented in the MRF initialization. What appears to be inadequately represented in the MRF realization is the strong gradient of θ_T and p_T immediately downstream of PV anomaly C. To the extent that the advection of lower (higher) values of $\theta_T(p_T)$ can be associated with deep ascent, vortex-tube stretching, and cyclogenesis in a conditionally unstable atmosphere, the misrepresentation of the structure of PV anomaly C in the MRF initialization at 12/12 (and 12 h-forecasts valid at the same time) may perhaps be one contributing factor to the relatively poor MRF forecasts of the incipient SS93 development.

A manually prepared vertical cross section of θ at 12/12 from Acapulco (ACA), Mexico, to Bismarck (BIS), North Dakota, is shown in Fig. 13. The leading edge of the northerlies marking the cold surge has

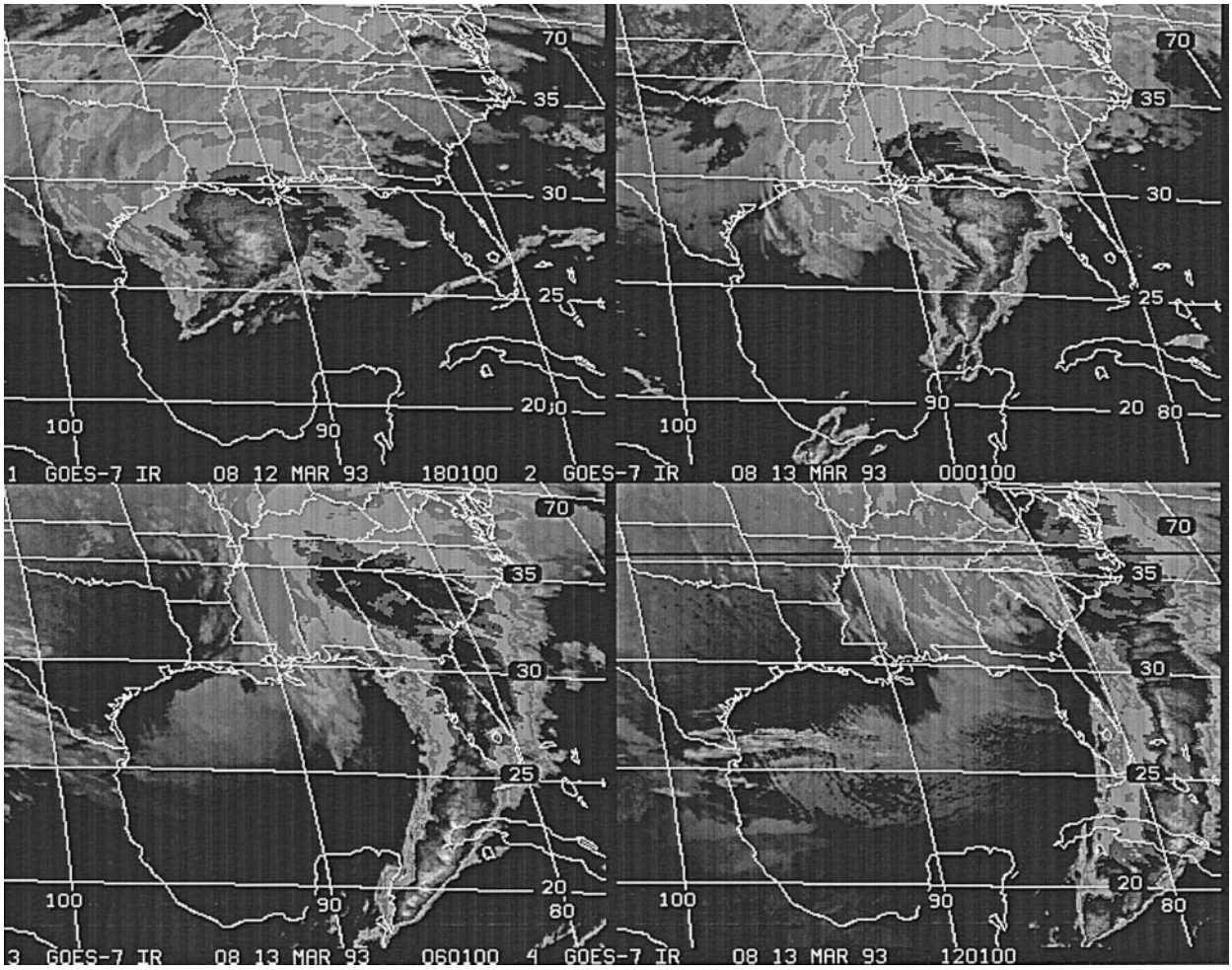

FIG. 6. (*Continued*)

reached CRP, but not BRO, at this time. The nose of the cold air is shallow and has the appearance of a density current (see Schultz et al. 1997). The vertical gradient of θ is near zero below 900 hPa just to the south of CRP, indicative of the very steep lapse rates in the lower troposphere ahead of the advancing cold surge. The stippling in Fig. 13 indicates regions of conditional instability (θ_e decreases upward) and shows the potential for deep convection in the boundary layer near and equatorward of BRO and in a shallow layer above the advancing low-level cold air from CRP to Little Rock, Arkansas (LZV).

The 1.5-PVU contour shown in Fig. 13 is derived from the 2.5° MRF-initialized DT and is interpolated to the sounding station locations. The position of the conventional lapse-rate-defined tropopause of the World Meteorological Organization (WMO) is readily apparent from the increased vertical gradient of θ extending from near 400 hPa at BIS to near 200 hPa at CRP in Fig. 13. The DT, defined by the 1.5-PVU surface, matches the conventional tropopause position reasonably well poleward of LCH. However, in the vicinity of BRO and CRP the DT lies in the 300–250-hPa range, lower than the conventional WMO tropopause position. The modest dip in the height of the DT in the vicinity of BRO is not an artifact of the cross-section location but reflects the approach of PV anomaly C immediately upstream (cf. Figs. 2a, 3b, and 3e). Note also that air on the DT with a value of $\theta_T \sim 330$ K near BRO resides over air with a θ_e of 335–345 K in the boundary layer near and equatorward of BRO (Fig. 5c), a manifestation of the potential for vigorous convection that is being realized by deep ascent (Figs. 3e, 4e) at 12/12. Finally, the uplifting of the 1.5-PVU contour between BRO and Mexico City (MEX), Mexico, coincides with the changeover from cyclonic to anticyclonic shear across the STJ.

4. Model representation of initial cyclogenesis

In this section we examine aspects of operational model performance during SS93. Although emphasis

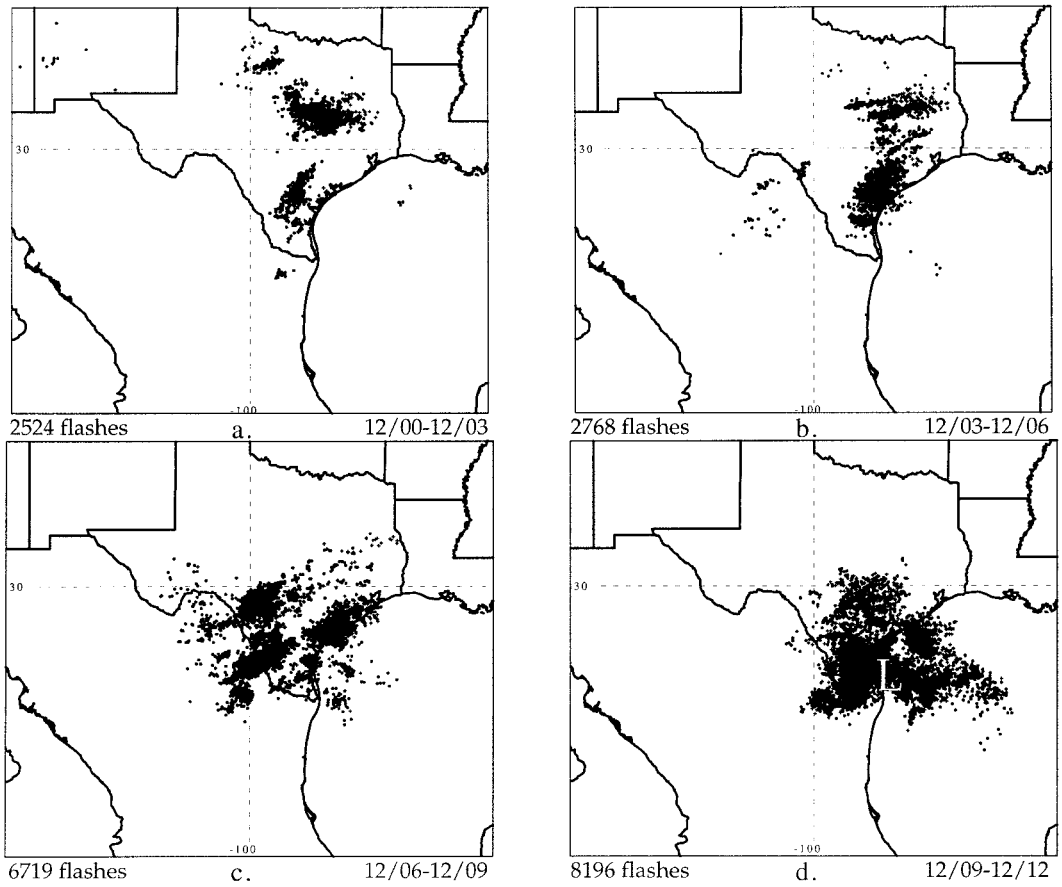

FIG. 7. Cloud-to-ground (CG) lightning flashes from the National Lightning Detection Network for 3-h periods (UTC/day; March 1993) ending (a) 03/12, (b) 06/12, (c) 09/12, (d) 12/12, and 6 h periods ending (e) 18/12, (f) 00/13, (g) 06/13, and (h) 12/13. Times correspond to Fig. 6. Number of CG flashes is plotted in the lower left-hand side of each panel. Position of surface cyclone is denoted by the "L" symbol.

will be placed on the MRF, the MRF analysis is supplemented with selected ECMWF model plots obtained courtesy of Adrian Simmons (1997, personal communication) for emphasis. The horizontal and vertical resolution of the MRF and ECMWF models was T126 (~100 km) and T213 (~60 km) and 18 and 31 levels, respectively.

a. Model overview

We had access to 12-h MRF forecast grids from the model runs initialized 00/12 and 12/12 and selected plots of 6-h ECMWF model forecasts initialized 12/11 and 12/12. We show for reference in Fig. 2b the observed and forecast surface cyclone track and forecast cyclone central pressure for these four model runs. These comparisons reveal: 1) the ECMWF model outperformed the MRF in terms of forecast cyclone intensity and track over the Gulf of Mexico although the ECMWF model still significantly underestimated the intensity of the initial cyclogenesis, and 2) the MRF forecast cyclone tracks were somewhat superior to the ECMWF forecasts along the northeast coast of the United States. In this section we will attempt to understand some of the possible reasons for the MRF behavior subject to the constraints imposed by the limited availability of gridded model forecast fields.

b. MRF initialization

The initialized MRF θ_e values at 850 hPa and the 850–700-hPa layer-averaged PV and winds from 12/00 to 13/00 are shown in Fig. 14a,b,c. Although the MRF θ_e values (Fig. 14a,b,c) cannot be compared directly with the surface observations (Fig. 5), the general patterns are comparable. At 00/12, the MRF depicts a north–south-oriented tongue of high-θ_e air at 850 hPa extending poleward to the lower Rio Grande Valley (Fig. 14a). By 12/12, significant cooling and drying has taken place in northern Texas while high θ_e values persist (and increase slightly) across southern Texas and northern Mexico (Fig. 14b). This leads to a strengthening of the CBZ (Fig. 5c) and a tightening of the 850-hPa θ_e gradient across southern Texas (Fig. 14b). How-

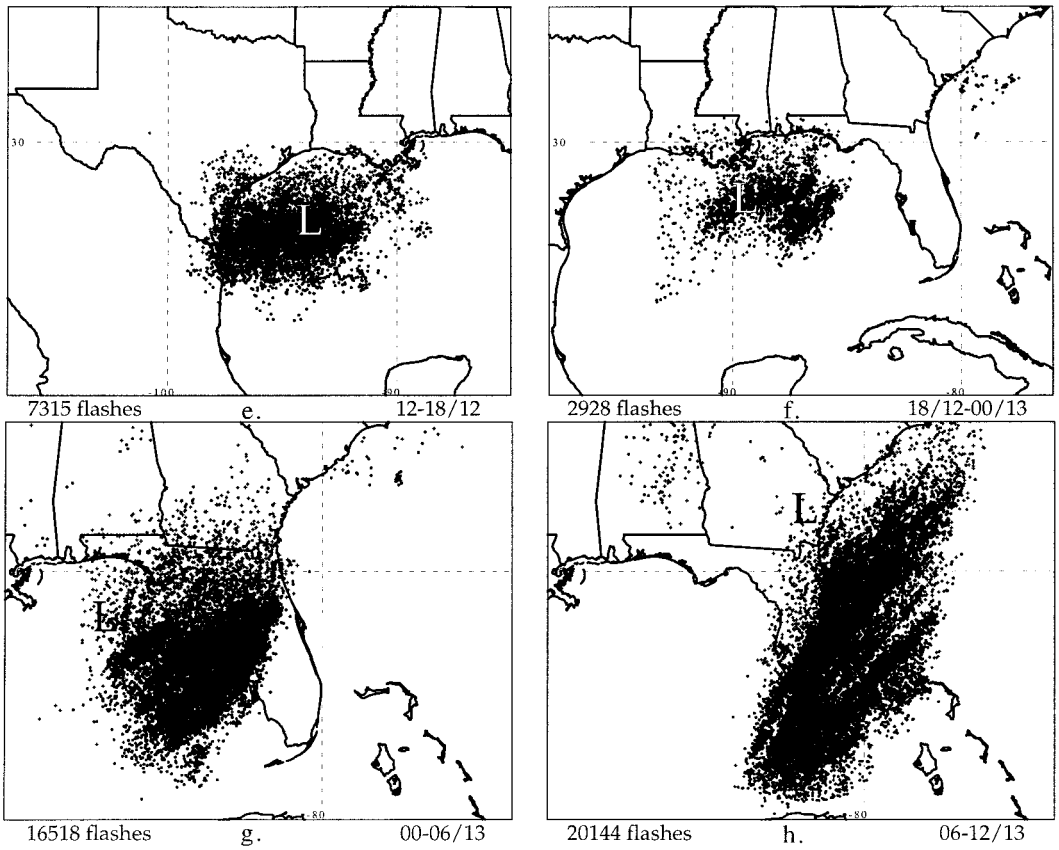

FIG. 7. (*Continued*)

ever, the developing cold surge in the MRF 850-hPa initialized θ_e patterns is too weak (Fig. 14b). Failure to simulate properly cold surges east of the Rockies is a common systematic error of NCEP operational models (e.g., Weiss 1992; Grumm and Gyakum 1986; Mesinger 1996). By 00/13 (Fig. 14c), the CBZ has shifted eastward in response to the continuing cold surge that reaches the Isthmus of Tehuantepec at this time (Schultz et al. 1997).

The 850–700-hPa layer-averaged PV and winds near the low-level cyclonic circulation center increase, especially after 12/12, as cyclogenesis commences (Figs. 14a,b,c). Comparison with Figs. 6, 8, and 9 reveals that rapid 850–700 hPa PV growth occurs approximately 12 h subsequent to the onset of deep convection and widespread precipitation. Given that the MRF initialization for 12/12 inadequately defines the low-level southeasterly flow along the Texas coast (see the CRP sounding in Fig. 12c), it is quite likely that the 850–700-hPa layer-averaged PV in the cyclogenetic environment is larger than initialized at 12/12. If so, the apparent time lag between diabatic heating and PV growth would be reduced. Further comparison with Figs. 3d,e,f also reveals that the growth of low-level PV occurs beneath decreasing p_T (and associated ridging on the DT), consistent with the expected development of an area of anticyclonic circulation above a deep region of extensive latent heat release.

The MRF initialized CAPE, CP, and 700-hPa vertical motion values are shown in Figs. 14d–i for the 24-h period ending 00/13. The MRF initialization is able to capture the observed high values of CAPE (computed by lifting a parcel from 1000 hPa) across southern Texas and the western Gulf of Mexico and the strong CAPE gradient across southern Texas at both 00/12 and 12/12. CAPE values exceed 3500 J kg^{-1} to the southeast of BRO through 12/12. By 00/13 the maximum CAPE is situated over the central Gulf of Mexico, equatorward of the low-level cyclone center (cf. Figs. 14h,i with Figs. 14b,c). Behind the cyclone, the cold-air surge through the western Gulf of Mexico is associated with sharply reduced CAPE values. The strongest 700-hPa ascent associated with PV anomaly C is situated across western Texas and eastern New Mexico at 00/12 (Fig 14d). By 12/12, the maximum 700-hPa ascent reaches the northwestern Gulf of Mexico and lies immediately poleward of the area of maximum CAPE (Fig. 14e) as surface development begins. As SS93 intensifies dramatically over the 12-h period ending 00/13, the maximum 700-hPa ascent almost doubles and continues to overlap significantly the poleward margin of the high-CAPE air (Figs. 14e,f,h,i).

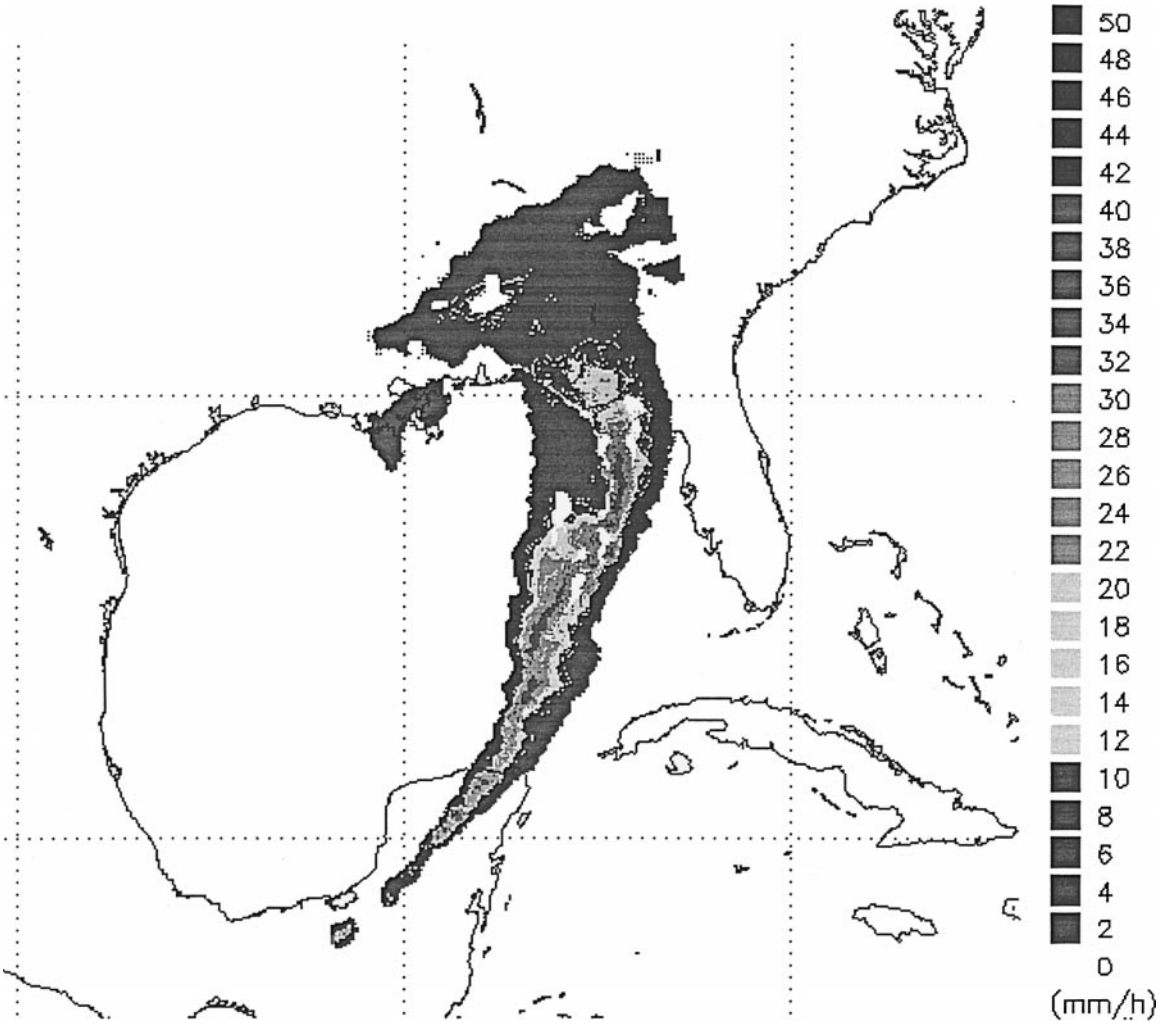

FIG. 8. Satellite-derived instantaneous precipitation rate (mm h^{-1}) according to the shaded scale at 0245 UTC March 13. Figure courtesy of R. Bauer of the National Snow and Ice Data Center/Defense Meteorological Satellite Program.

c. MRF forecast errors

The results from section 3a suggest that the MRF initialization is adequately capturing the observed mass and wind fields at 00/12 associated with the precyclogenetic phase of SS93 (Figs. 11a,b) but is inadequate at later times as cyclogenesis proceeds in the presence of deep convection (Figs. 12a,b,c). These findings suggest that inadequate parameterized model physics may be contributing to the poor forecasts of the incipient SS93 cyclogenesis. In this section we will show that the MRF forecasts are unable to simulate properly the bulk effects of cumulus convection on the troposphere. To help identify the errors in the forecast fields, MRF initialized fields are subtracted from the forecast fields at the corresponding verification time (forecast − initialization). Here we consider the differences in the 12-h forecast verifying 12/12 and the 24-h and 12-h forecasts verifying 00/13.

Figure 15 shows maps of MRF forecast θ_T, p_T, winds, θ_T advection, and vertical velocity at these times and Fig. 16 shows the corresponding forecast errors. At 12/12 the 12-h MRF θ_T forecast averages 5–10 K too low. Similarly, the 12-h MRF p_T forecast is too high by 25–50 hPa along the Texas coast northeastward to Tennessee (cf. Figs. 3d, 15d, 16d). Taken together these results imply that the MRF 12-h forecast DT is too low and too cold (θ sense) in a broad northeast–southwest-oriented band ahead of PV anomaly C. The cyclonic wind error pattern over southern Louisiana indicates that the southwesterly flow poleward of the developing convection and southeast of PV anomaly A is too weak in a broad anticyclonic arc from Texas to West Virginia in the 12-h MRF DT forecast for 12/12. Consequently, the developing jet on the forward side of the trough containing PV anomaly A is too weak and the STJ over the Gulf of Mexico is overestimated somewhat. Note also that by comparing Figs. 3e, 15d, and 16d, we see that the 12-h vertical motion forecast is too weak and situated too far to the east of the cyclogenetic region.

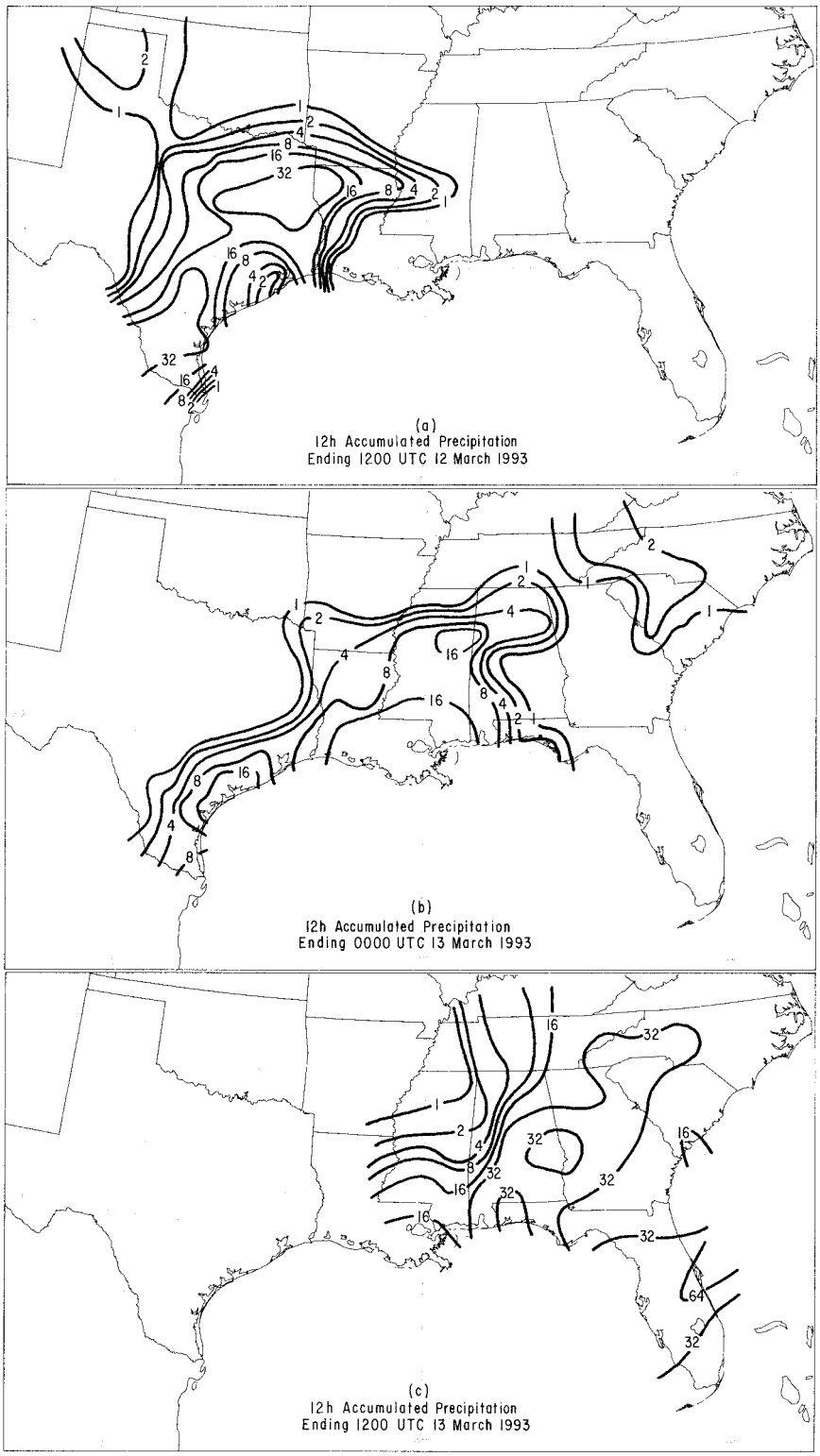

FIG. 9. Observed 12-h accumulated precipitation (solid, contours every 1, 2, 4, 8, 16, 32, and 64 mm) ending (a) 1200 UTC 12 March 1993, (b) 0000 UTC 13 March 1993, and (c) 1200 UTC 13 March 1993.

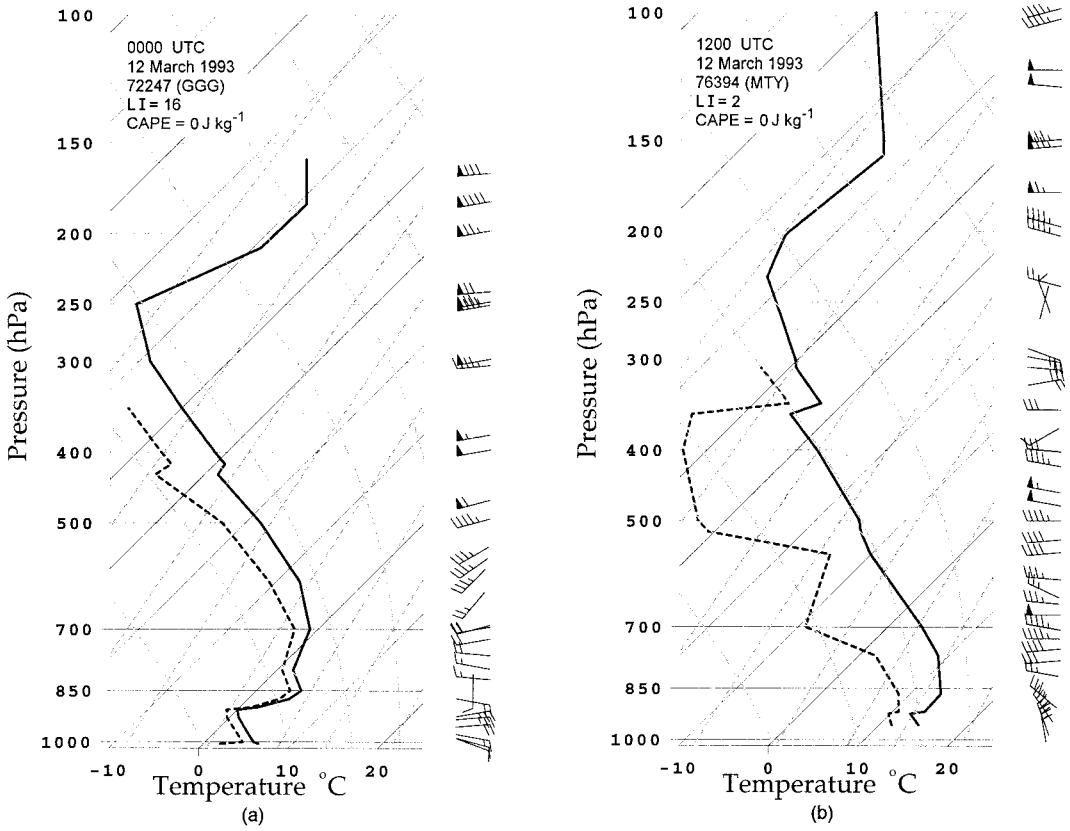

FIG. 10. Skew *T*–log*p* format temperature (°C, solid line), dewpoint temperature (°C, dashed line), and wind profiles (m s^{-1}) at (a) 0000 UTC 12 March 1993 for Longview, Texas (GGG 72247), and (b) 1200 UTC 12 March 1993 for Monterrey, Mexico (MTY 76394).

These error patterns persist and amplify in the 24-h and 12-h forecasts verifying 00/13 (Figs. 15b,c,e,f and 16b,c,e,f). The poleward bulge in the θ_T contours across the southeastern United States is greatly underestimated by the 24-h MRF forecast (cf. Figs. 3c and 15b,c). The largest θ_T error occurs along the Alabama–Georgia border where the 24-h MRF forecast θ_T value of 330 K (Fig. 15b) is more than 30 K too low (Fig. 16b). Similarly, the forecast values of p_T average more than 75 hPa too high over the southeastern United States (Figs. 16e,f). Comparison of the 24-h DT forecast and initialized winds at 00/13 (Figs. 3c and 15b) reveals the much larger anticyclonic curvature in the initialized winds over the southeastern United States. This area of enhanced anticyclonic flow is associated with a more elevated and warmer (θ sense) initialized DT. Note also that the winds on the DT in the 24-h MRF forecast (Fig. 12b) are roughly parallel to the θ_T isentropes over the southeastern United States, suggestive of near-adiabatic conditions in the model DT forecasts, in comparison to the wind–θ_T configuration on the initialized DT.

Further comparison of Figs. 3c,f and 15b,e reveals that the unforecast nonconservation of θ_T prevents the MRF model from capturing the significant advection of lower values of θ_T (equivalent to the positive advection of PV on the DT) over the rapidly intensifying storm center by 00/13. The 24-h MRF DT forecast for 00/13 is unable to capture this favorable cyclogenesis pattern (Figs. 15b,e and 16b,e). Figures 16b,e further reveal that the MRF 24-h forecast also continues to fail to capture the rapidly strengthening southwesterly jet ahead of PV anomaly A from Arkansas northeastward to Ohio. This jet is marked by an extended two-dimensional gradient of θ_T and p_T, created by higher values of θ_T and lower values of p_T associated with the convection described above, over the southeastern United States in the initialized fields. Clearly, the effective redevelopment of the jet from the west to the east side of the deepening trough containing PV anomaly A is strongly linked to a precipitation (convective and stratiform)-modified DT evolution over the southeastern United States. In this regard, there is interaction between PV anomalies A and C prior to their formal merger by 00/14 (Bosart et al. 1996). Finally, we note that the above error patterns, although reduced in the 12-h forecasts verifying 00/13 (Figs. 16c,f), are comparable in scope to the 24-h forecasts verifying the same time.

The MRF forecast 850-hPa θ_e, 850-700-hPa layer-averaged PV, and wind fields for the 12-h and 24-h forecasts verifying 12/12 and 00/13, respectively, and

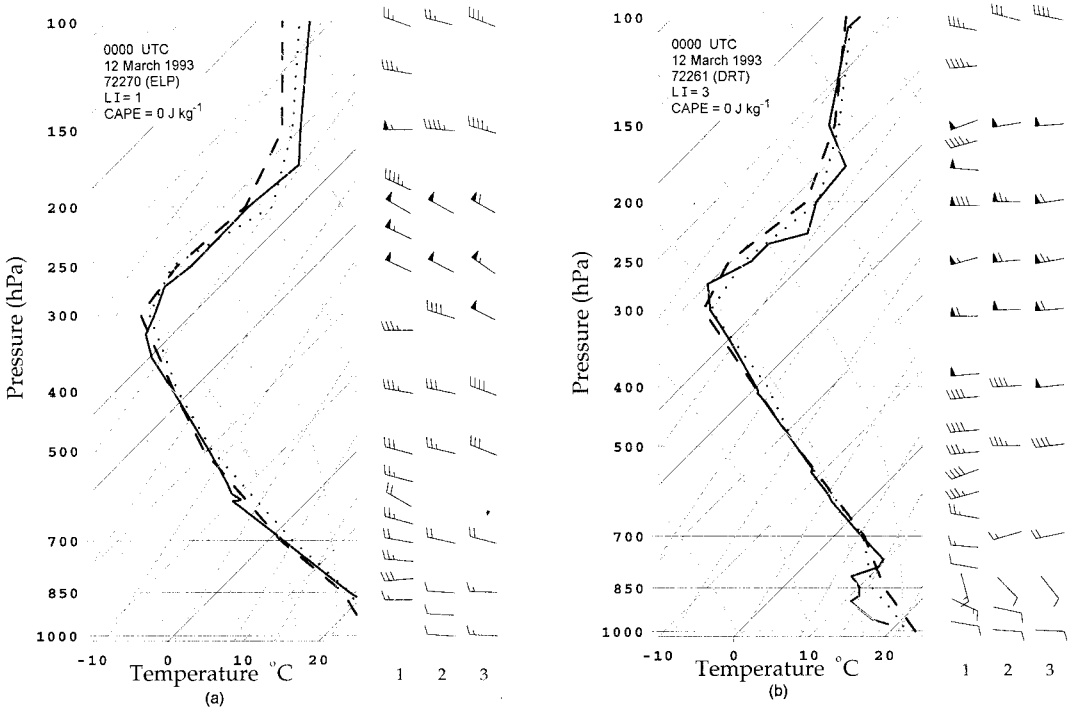

FIG. 11. As in Fig. 10 except for observed (solid), ECMWF uninitialized (dotted), and MRF initialized (dashed) temperatures (°C) and winds (m s^{-1}, wind position 1: observed, position 2: ECMWF, and position 3: MRF) at 0000 UTC 12 March 1993 for (a) El Paso, Texas (ELP 72270), and (b) Del Rio, Texas (DRT 72261).

the 12-h forecast verifying 00/13 are presented in Figs. 17a,b,c. Figures 17d,e,f show the corresponding forecast difference fields. The difference maps reveal that the poleward extent of the high-θ_e surge over the northeastern Gulf of Mexico into northern Florida ahead of the developing cyclone is underestimated, consistent with the MRF failure to develop a strong enough cyclonic circulation over the Gulf of Mexico subsequent to 12/12. This situation is readily apparent by comparing the model forecast 850-700-hPa layer-averaged winds in Figs. 17a,b,c with the model initialized winds for the same time periods in Figs. 14a,b,c and the forecast minus initialized 850-700-hPa layer-averaged PV and wind fields displayed in Figs. 17d,e,f. Comparison of Figs. 17e,f with Fig. 14c shows that the MRF 12-h and 24-h forecasts verifying 00/13 significantly underestimate the strength of the mean 850–700-hPa low-level PV anomaly over the northern Gulf of Mexico. The presence of an anticyclonic forecast wind error pattern (Figs. 17e,f) that is collocated with the negative PV forecast error over the northern Gulf of Mexico confirms this interpretation. Note also that the equatorward advection of cold air in the wake of the underforecast cyclogenesis is underestimated at all forecast projections.

A similar set of MRF model forecasts of CAPE and 700-hPa vertical velocity are presented in Figs. 18a,b,c. Comparison of Figs. 18a,b,c with Figs. 14d,e,f reveals the overforecast of CAPE and the overlap between high CAPE values and 700-hPa ascent in the vicinity of the developing cyclone for all forecast projections. Also of interest in Figs. 18a,b,c is the failure of the MRF forecasts to spread vigorous 700-hPa ascent across the Florida panhandle in advance of the intensifying cyclone by 00/13 (cf. Figs. 18b,c and Fig. 14c). Likewise, the CP is poorly represented across much of the southeastern United States by 00/13 where CP errors exceed −30 K (−25 K) in the 24-h (12-h) forecasts verifying 00/13 (not shown but note that CP errors resemble the θ_T errors shown in Figs. 16a,b,c). These CP errors are linked to the MRF failure to adequately increase θ_T and decrease p_T as the DT is lifted and warmed downshear of the large area of the convective and stratiform precipitation over the Gulf of Mexico and along the coast of the Gulf of Mexico (recall Figs. 3c,f, Figs. 15b,c,e,f, and Figs. 16b,c,e,f).

The MRF 12-h total, large-scale and convective precipitation forecasts are shown in Fig. 19 for the 24–36-h, 12–24-h, and 24–36-h periods verifying 12/12, 00/13, and 12/13, respectively (note that MRF precipitation forecasts are archived at NCAR for the 0000 UTC model cycle only). Comparison of Figs. 19a,b,c with Fig. 9 reveals that the MRF generally underforecasts precipitation along the Gulf Coast states, notable examples include Texas by 12/12 and central Florida by 12/13. The Texas error arises because the areal extent of MRF forecast convective precipitation (Fig. 19g) is too small and the forecast amount is too light and displaced too far east over the Gulf of Mexico based upon a comparison with the lightning and satellite data (Figs. 6–8). Clearly, the massive convective

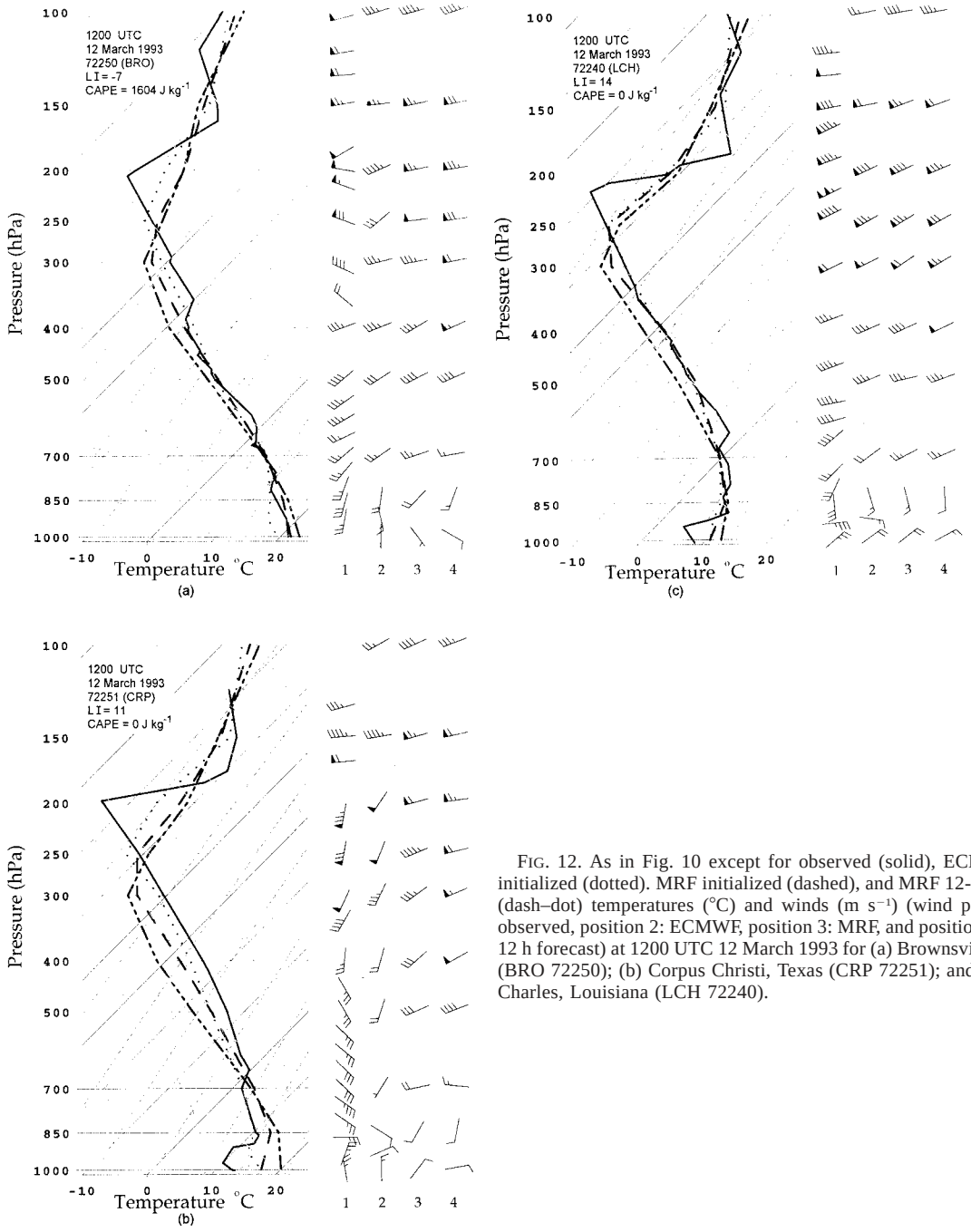

FIG. 12. As in Fig. 10 except for observed (solid), ECMWF uninitialized (dotted). MRF initialized (dashed), and MRF 12-h forecast (dash–dot) temperatures (°C) and winds (m s^{-1}) (wind position 1: observed, position 2: ECMWF, position 3: MRF, and position 4: MRF 12 h forecast) at 1200 UTC 12 March 1993 for (a) Brownsville, Texas (BRO 72250); (b) Corpus Christi, Texas (CRP 72251); and (c) Lake Charles, Louisiana (LCH 72240).

outbreak that heralds the incipient SS93 cyclogenesis is not replicated in the MRF forecasts, a problem that persists as the convection spreads eastward across the Gulf of Mexico and Florida.

d. Influences of convection

A comparison of the MRF and ECMWF DT analyses (Figs. 3 and 4) and the tracks of the MRF and ECMWF forecast cyclone (Fig. 2b) suggests that the diabatic heating effects associated with convection over the northwestern Gulf of Mexico was better forecast in the ECMWF model during the development phase of SS93. To help bolster this assertion, we show in Fig. 20 maps of ECMWF forecast convective and large-scale precipitation for 6-h periods ending 12/12, 18/12, and 00/13 based upon the model run initialized 12/11. For comparison purposes an updated 6-h forecast ending 18/12 from the model run initialized 24-h later at 12/12 is also included in Fig. 20. These results should be compared

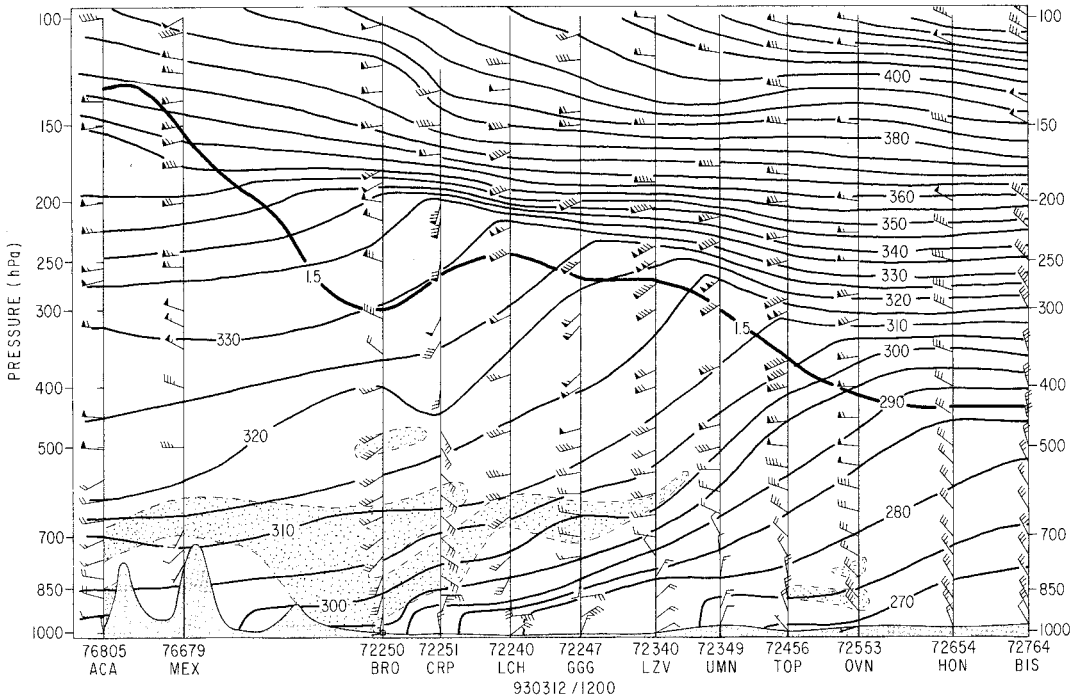

FIG. 13. Cross section from Acapulco, Mexico (ACA 76805), to Bismarck, North Dakota (BIS 72764), at 1200 UTC 12 March 1993 (see Fig. 2a for station locations) of potential temperature θ (solid, every 5 K) and winds (m s^{-1}). Stippled area denotes region of conditional instability. Winds plotted according to the convention in Fig. 3. Bold solid lines denote the PVU = 1.5 contour from the MRF (Fig. 3).

to the MRF forecast precipitation (only 12-h periods are available) given in Fig. 19.

In general the ECMWF precipitation forecasts from the run initialized 12/11 show convective rains (4–8 mm per 6 h) beginning prior to 12/12 over Texas (Fig. 20a). This convective rain area intensifies (>32 mm per 6 h) as it moves eastward across the northern Gulf of Mexico through 00/13 (Figs. 20b,c). Note also the tendency for the convective rain area to bulge equatorward somewhat by 00/13 in agreement with the observed squall development (Fig. 9) and reflected even better in the comparable forecasts initialized 12/12 (not shown). The ECMWF 6-h forecast verifying 18/12 from the updated 12/12 model cycle shows that the convective precipitation is more intense and displaced poleward from the comparable earlier model run (Fig. 20d). This trend continues for the forecasts beyond 18/12 (not shown). Note also the substantial overlap between the convective and large-scale precipitation in the ECMWF forecasts (Figs. 20e–h) in comparison to the small area of overlap in the MRF forecasts. Comparison of Figs. 19 and 20 with the observations also shows that the MRF falsely predicts convective rains equatorward of Louisiana and fails to predict the developing convective precipitation over Texas by 12/12.

To help assess the impact of diabatic heating associated with latent heat release on the model forecasts, we show maps of 250-hPa heights and winds for the 24- and 36-h ECMWF and 12- and 24-h MRF forecasts verifying 12/12 and 00/13 in Fig. 21. Comparison with Figs. 2–4 shows that although both model forecasts resolve PV anomalies A and C, the signature of these PV anomalies is better defined in the higher resolution ECMWF forecasts. The differences in the wind and height relationships between the two models are suggestive, however. Note the cross-contour flow directed toward higher heights in the northwesterly flow of the jet exit region upshear of PV anomaly C in the ECMWF forecast (Figs. 21a,b). This flow configuration is suggestive of a deepening trough and is not as evident in the coarser resolution MRF forecasts at the later model initialization time (Figs. 21c,d). Note also the 250-hPa heights are forecast to decrease from the Gulf of Mexico poleward to the Great Lakes in the 12-h period ending 00/13, indicative of the deepening large-scale trough in which PV anomalies A and C are embedded.

Of equal or possibly greater significance is the appreciable cross-contour flow toward lower heights seen to develop in the 36-h ECMWF 250-hPa forecast verifying 00/13 (Fig. 21b). This developing area of large cross-contour flow toward lower heights, situated downshear of the rapidly developing forecast precipitation shield over the Gulf of Mexico, feeds the developing PFJ on the forward side of PV anomaly A. This developing surge of upper-tropospheric outflow from the northern part of the Gulf of Mexico is also consistent with the observed increases (decreases) of θ_T (p_T) on the DT over the southeastern United States shown in

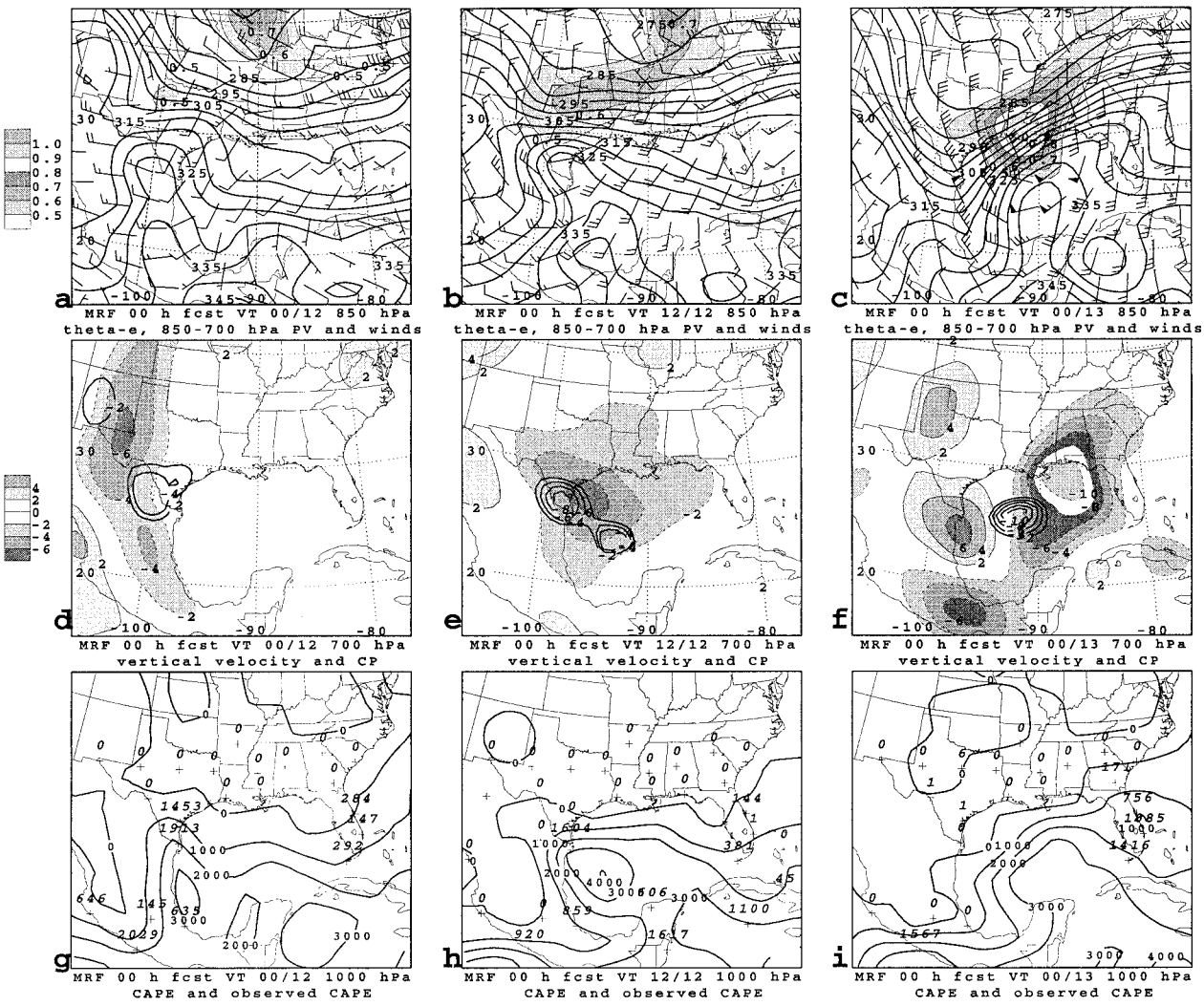

FIG. 14. (a)–(c) MRF initialized 850-hPa equivalent potential temperature (solid, every 5 K) and 700–850-hPa layer-averaged PV (shading interval 0.1 PVU, scaled at left; see Fig. 3) and winds (m s^{-1}) at (UTC/day; March 1993) (a) 00/12, (b) 12/12, and (c) 00/13. (d)–(f) MRF-initialized CP (solid contours every 2 units for values less than or equal to 0) and 700-hPa vertical velocity (every 2 hPa s^{-1}); shaded by scale to left with ascent (descent) regions outlined by thin dashed (solid) lines at (d) 00/12, (e) 12/12, and (f) 00/13 March 1993. (g)–(i) MRF-initialized CAPE (contours of 0, 500, 1000 and every 1000 J kg^{-1} thereafter) with observed CAPE values plotted directly at sounding stations. Times as in (d)–(f).

Fig. 4. These circulation signatures are even more pronounced in the ECMWF 250-hPa forecasts initialized 24-h later at 12/12 (not shown) but are somewhat weaker in the MRF forecasts from 00/12 (Fig. 21d). These subtle model differences suggest that upper-tropospheric outflow from the extensive area of diabatic heating over the Gulf of Mexico is less well defined in the MRF, a conclusion reinforced by a comparison of Figs. 3 and 4.

To help reinforce this last point we display in Fig. 22 identical forecasts to Fig. 21 except for 500-hPa heights and vorticity. Comparison with Fig. 2a shows that PV anomalies A and C are both resolved in the ECMWF and MRF forecasts verifying 12/12 and 00/13. The evolution of PV anomaly C in the 12-h period ending 00/13 suggests that its behavior is governed mostly by simple advective processes in the MRF forecasts (Figs. 22a,b) whereas the new cyclonic vorticity development within the poleward periphery of PV anomaly C in the ECMWF forecasts (Fig. 22c,d) is more consistent with local cyclonic vorticity generation. Support for this last assertion is also provided by comparison of Figs. 22c,d and Figs. 20c,g, which shows that the new cyclonic vorticity growth at 500 hPa lies immediately downshear of a combined region of appreciable convective and large-scale precipitation.

e. Low-level thermal structure and oceanic heat fluxes

Surface sensible and latent heat fluxes in the vicinity of SS93 during its developmental phase over the Gulf

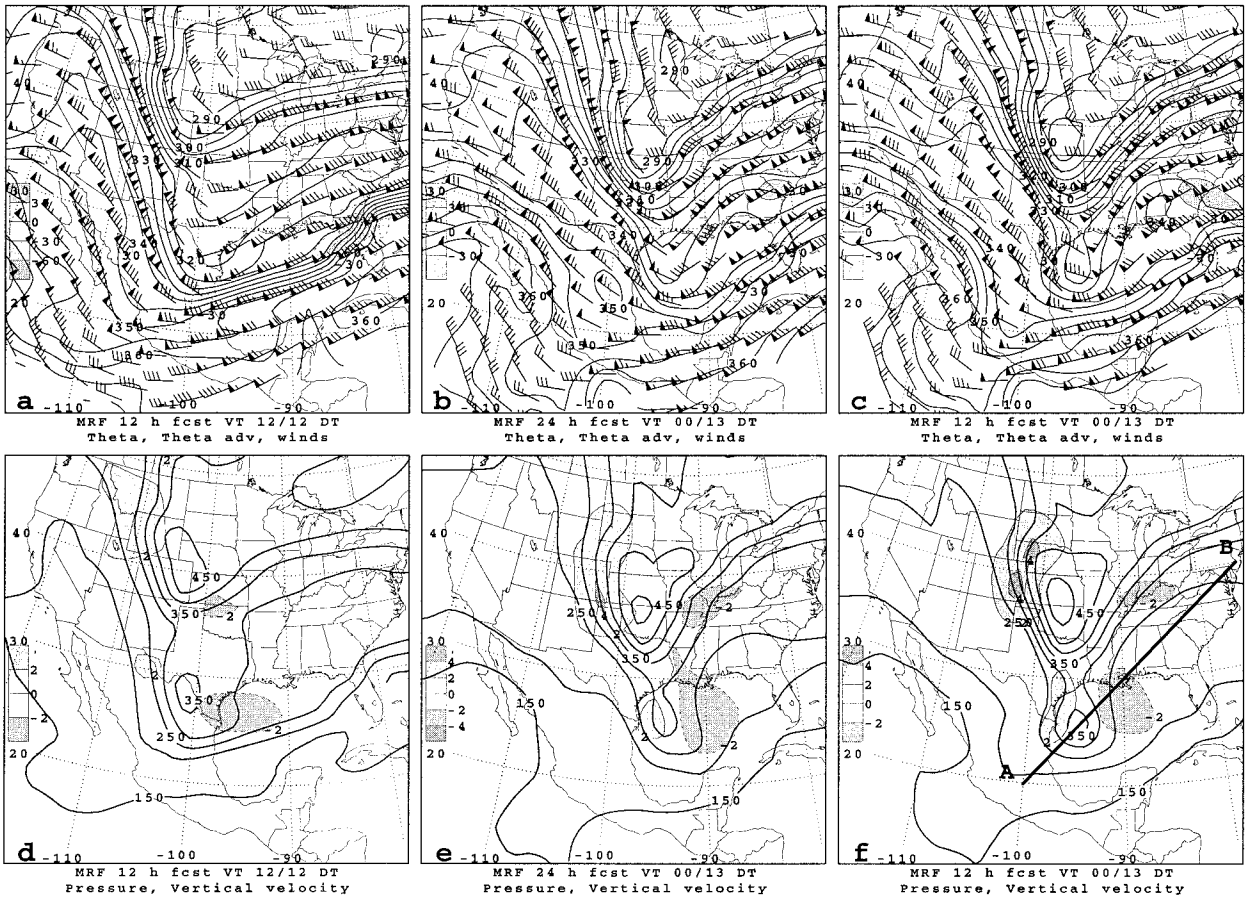

FIG. 15. As in Fig. 3 except for (a) and (d) 12-h MRF forecast verifying 1200 UTC 12 March 1993, (b) and (e) 24-h MRF forecast verifying 0000 UTC 13 March 1993, and (c) and (f) 12-h forecast verifying 0000 UTC 13 March 1993. Cross-sectional line for Fig. 20 is shown in panel (f).

of Mexico averaged 50–150 W m^{-2} in both the MRF and ECMWF model forecasts (not shown) with the larger values being forecast by the higher resolution ECMWF model. These flux values increase to more than 1000 W m^{-2} over the northwestern Gulf of Mexico subsequent to 00/13 as cold air from the continent in the wake of SS93 was advected equatorward (not shown). However, the forecast heat fluxes appear to be underestimated in comparison to estimates made at individual ship reporting locations using the standard bulk aerodynamic formulas in the northerly and northeasterly inflow poleward and ahead of the track of the intensifying storm center. Marine observations in the 12-h period ending 00/13 (see, e.g., Kocin et al. 1995; their Figs. 9 and 11) reveal that 20–30 m s^{-1} northerlies are common at oil rig locations south of Louisiana along with air and dewpoint temperatures in the 10°–16°C range. With SSTs between 18° and 21°C in this region, combined surface sensible and latent heat fluxes of 500–1500 W m^{-2} are computed (not shown) in the storm-inflow region.

The heat flux discrepancy between the observations and model forecasts can be attributed to 1) both weaker wind speed and weaker low-level thermal gradient forecasts in the models (especially the MRF), and 2) an underestimate of the SST over the Gulf of Mexico in the models, especially the MRF. The weaker forecast winds can be associated with underforecasts of the cyclogenesis intensity over the Gulf of Mexico (recall Fig. 2). Similarly, the weaker model forecast thermal gradients can be associated with the model failure to adequately represent the observed cooling over the northern Gulf of Mexico as the strengthening northerly flow in the poleward semicircle of the rapidly deepening cyclone allows cold continental air to reach the storm inflow region quicker than forecast (not shown). This problem is exacerbated in the MRF where the forecast cyclone tracks eastward across the Gulf of Mexico well equatorward of the main (and anomalously weak) baroclinic zone (Fig. 2b).

The SST analysis problem during SS93 is discussed in Gilhousen (1994). He reproduced the National Hurricane Center's (NHC) sea surface thermal analysis (his Fig. 10) to reveal the existence of a positive SST anomaly of about 2°–3°C associated with a tongue of warm water between 94° and 96°W where an SST of 23°C is

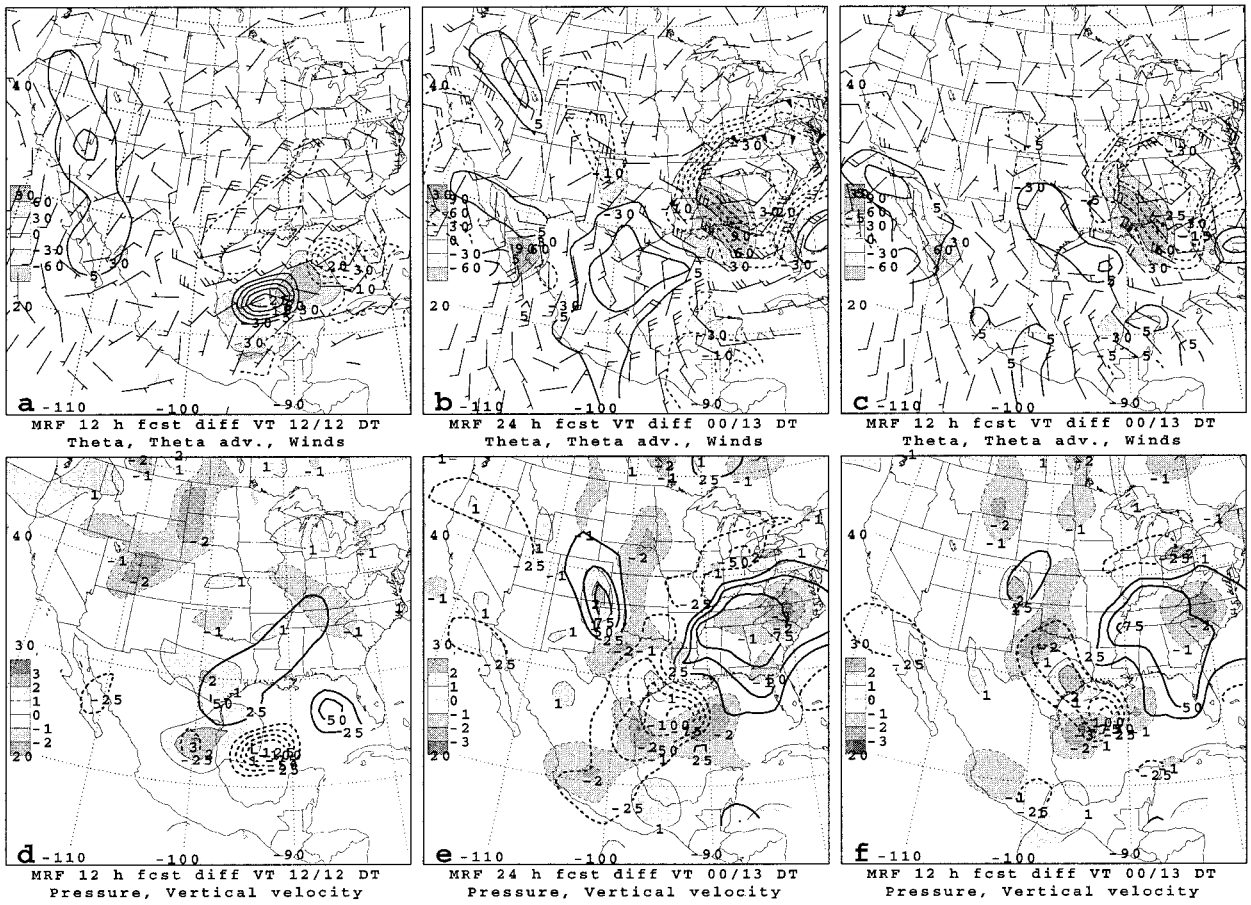

FIG. 16. As in Figs. 3 and 15 except for difference fields (forecast minus initialized) of DT winds (m s^{-1}; Fig. 3) and θ_T (solid/dashed for positive/negative differences, every 5 K) for (a), (b), and (c) and p_T (solid/dashed for positive/negative differences, every 25 hPa) for (d), (e), and (f). Shading interval of 30 K (12 h)$^{-1}$ (left) for potential temperature advection in panels (a), (b), and (c), and 1 hPa s^{-1} for vertical velocity in panels (d), (e), and (f). Thin solid (dashed) contours around shaded areas denote positive (negative) values. MRF forecasts are 12 h verifying 1200 UTC 12 March 1993 (a) and (d); 24 h verifying 0000 UTC 13 March 1993 (b) and (e) and 12 h verifying 0000 UTC 13 March 1993 (c) and (f).

observed as far poleward as 27°N (see also Walker 1993). This warm tongue was part of a warm eddy (named the ''Eddy Vasquez'' by oceanographers), sometimes called an oceanic ring, that had broken off from the Loop Current in the eastern Gulf of Mexico in October 1992. (Similar warm eddies with length scales of approximately 100–200 km are frequently observed along the Gulf Stream. Roebber (1989) used a simple analytical quasigeostrophic model to demonstrate that warm oceanic rings could possibly impact cyclogenesis intensity in situations where the trajectory of a mobile cyclone intersected the warm ring. Bosart et al. (1995), in an investigation of a case of Gulf Stream cyclogenesis, suggested that the cyclone may have experienced an accelerated rate of deepening as it traversed a 200–300-km poleward meander of the Gulf Stream.) The NHC positive SST anomaly is significantly underestimated in the MRF coarse-mesh SST analysis shown in Fig. 2b, suggestive that the heat flux estimates computed from the MRF forecasts are likely to underestimate the actual heat fluxes, especially over the northwestern Gulf of Mexico (not shown). Gilhousen (1994) also noted that the NHC SST analysis was too cold by about 1°–2°C in the vicinity of bouys 42019, 42020, and PTAT2 (Fig. 2b) immediately preceding SS93 development on the basis of the frequently reported SSTs from these locations. Given that 1°C negative SST anomalies were reported in the immediate coastal waters from CRP eastward to the Mississippi Delta, an anomalously strong SST gradient over the northwestern Gulf of Mexico (estimated anomaly SST gradient is approximately 4°C (75 km)$^{-1}$ near 28.0°N, 95.0°W from Fig. 10b of Gilhousen 1994) may have also acted to help enhance the low-level atmospheric baroclinicity that was tapped by PV anomaly C during the initial SS93 cyclogenesis.

In addition to the enhanced SST gradient, the atmospheric baroclinic zone in which SS93 develops is also quite intense. Gilhousen (1994) showed that buoys 42019, 42020, and PTAT2 captured the incipient SS93 development in the vicinity of 12/12. The developing

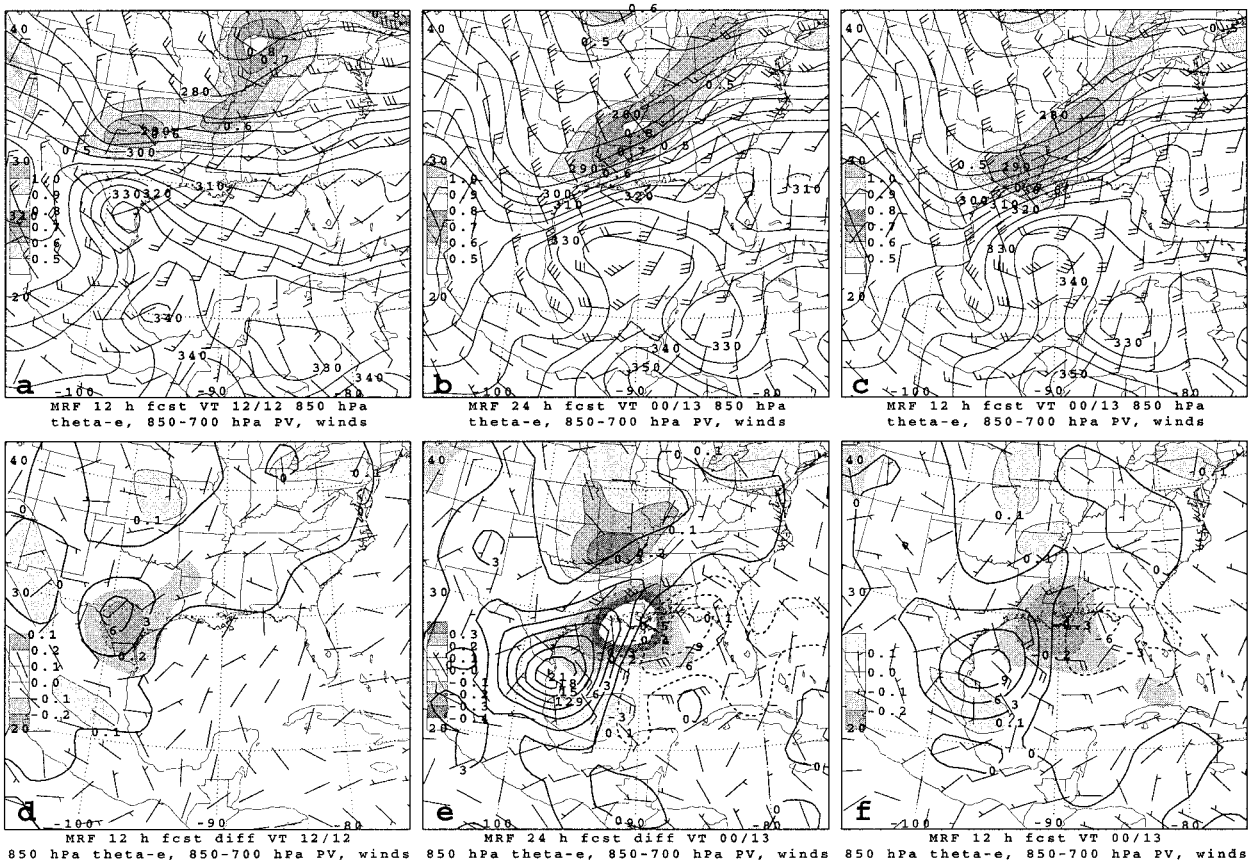

FIG. 17. Panels (a), (b), and (c) as in Figs. 14 (a), (b), and (c) except for 12-h MRF forecast verifying 1200 UTC 12 March 1993 (a), 24-h MRF forecast verifying 0000 UTC 13 March 1993 (b), and 12-h MRF forecast verifying 0000 UTC 13 March 1993 (c). Panels (d), (e), and (f) show difference (forecast minus initialized) fields of 850-hPa equivalent potential temperature (solid, every 3 K except dashed contours for negative values), 700–850-hPa layer-averaged PV (shaded, every 0.1 PVU, scale at left), and winds, (m s^{-1}, according to Fig. 3).

storm circulation center clearly passed poleward (equatorward) of buoy 42020 (42019) on the basis of the veering (backing) of the observed hourly winds (Gilhousen 1994; his Fig. 3). Sustained winds were in the 15–20 m s^{-1} range (buoy anemometer height approximately 5 m) with the strongest winds occurring as northerlies immediately behind the storm. Given that temperatures measured by 42019, 42020, and PTAT2 differed by about 10°C (average station spacing of about 100–200 km), it is apparent that the cyclonic circulation center that passed through this network was embedded in a region of appreciable baroclinicity. Equally important, this strong baroclinic zone defined the poleward limit of the high-θ_e (~340 K) air mass at the surface and coincided with the anomalously strong SST gradient described in the previous paragraph.

5. Concluding discussion and perspective

a. Storm overview

This paper has presented an analysis of the incipient stages of the remarkable Superstorm '93 (SS93) cyclogenesis event of 12–14 March 1993 while the storm was over the Gulf of Mexico. As shown by, for example, Sanders and Gyakum (1980) and Roebber (1984), the Gulf of Mexico, a well-known source region for cyclones, is not a climatologically favored area for explosive extratropical cyclone development. The unique nature of the SS93 cyclogenesis event at low latitudes was confirmed by our analysis showing that SS93 was the deepest extratropical cyclone ever observed over the Gulf of Mexico during the 1957–96 period.

Bosart et al. (1996) suggest that the unique aspect of the SS93 development could be attributed to the lateral and vertical interaction of long-lived individual PV anomalies (shown to have circumnavigated the Northern Hemisphere prior to the SS93 cyclogenesis) embedded within separate branches of the westerlies. These PV anomalies in turn interacted with an exceptionally unstable air mass over the northwestern Gulf of Mexico. On the larger scale, an amplifying western North American ridge and downstream trough (consistent with the positive phase of the Pacific–North American (PNA) flow pattern; Wallace and Gutzler 1981) resulted in the

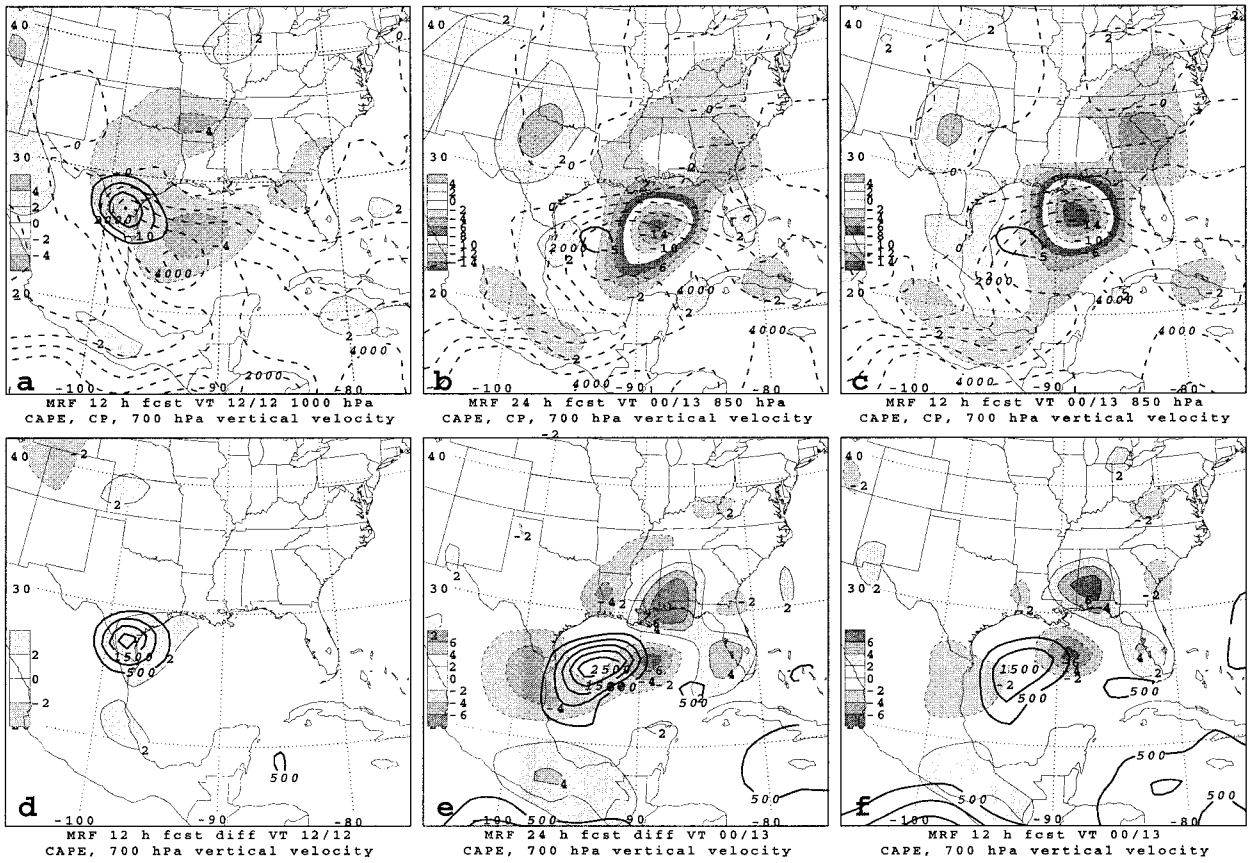

FIG. 18. Panels (a), (b), and (c) as in Figs. 14 (d), (e), and (f) except for (a) 12-h MRF forecast verifying 1200 UTC 12 March 1993, (b) 24-h MRF forecast verifying 0000 UTC 13 March 1993, and (c) 12-h MRF forecast verifying 0000 UTC 13 March 1993. Panels (d), (e), and (f) show difference fields (forecast minus initialized) of CAPE (thin solid, contours of 0, 500, 1000, and every 1000 J kg^{-1} thereafter), and vertical velocity [shaded by scale at left every 2 hPa s^{-1} with positive (negative) difference regions outlined by thin solid (dashed) lines around the shaded areas].

establishment of a confluent flow pattern across the Rockies. This flow regime favored the transport of arctic air equatorward toward the western Gulf of Mexico east of the Rockies. The presence of the Rockies is crucial to the cyclogenesis process because lee troughing in advance of the PV anomaly in the southern branch of the westerlies favors the poleward advection of warm, moist unstable air into southeastern Texas and adjacent regions.

Our DT analysis confirms the interpretation of Bosart et al. (1996) that the incipient SS93 cyclogenesis is triggered by a potent PV anomaly embedded in the southern branch of the westerlies (PV anomaly C in Bosart et al. 1996; Figs. 2a and 3 here) as it crosses extreme northern Mexico and approaches the Gulf of Mexico. Cyclogenesis immediately offshore of coastal southeastern Texas occurs in a low-level environment increasingly warmed and moistened by a persistent southeasterly flow over the western Gulf of Mexico as surface pressures remain relatively low over the northeastern Mexican plateau. The arrival of PV anomaly C is associated with the advection of lower values of θ_T over the northwestern Gulf of Mexico as the DT is lowered. The resulting destabilization of the troposphere, made explicit by the generation of negative values of the CP index, leads to the eruption of deep convection in the cyclogenetic environment in response to ascent ahead of PV anomaly C. A comparison of the MRF initialized and forecast DT fields of potential temperature, pressure, wind, and vertical motion for the 24-h period ending 00/13 reveals that the intensity of PV anomaly C is underestimated over the Gulf of Mexico in the MRF 12-h and 24-h forecasts verifying 12/12 and 00/13, respectively. A direct consequence of the underestimation of PV anomaly C is that the forecast cyclogenesis over the northwestern Gulf of Mexico is significantly weaker in comparison to observations (Fig. 3).

b. Model failure: Convection

We have presented evidence that the MRF failure to simulate properly the incipient SS93 cyclogenesis over the Gulf of Mexico can be linked to the inability of the

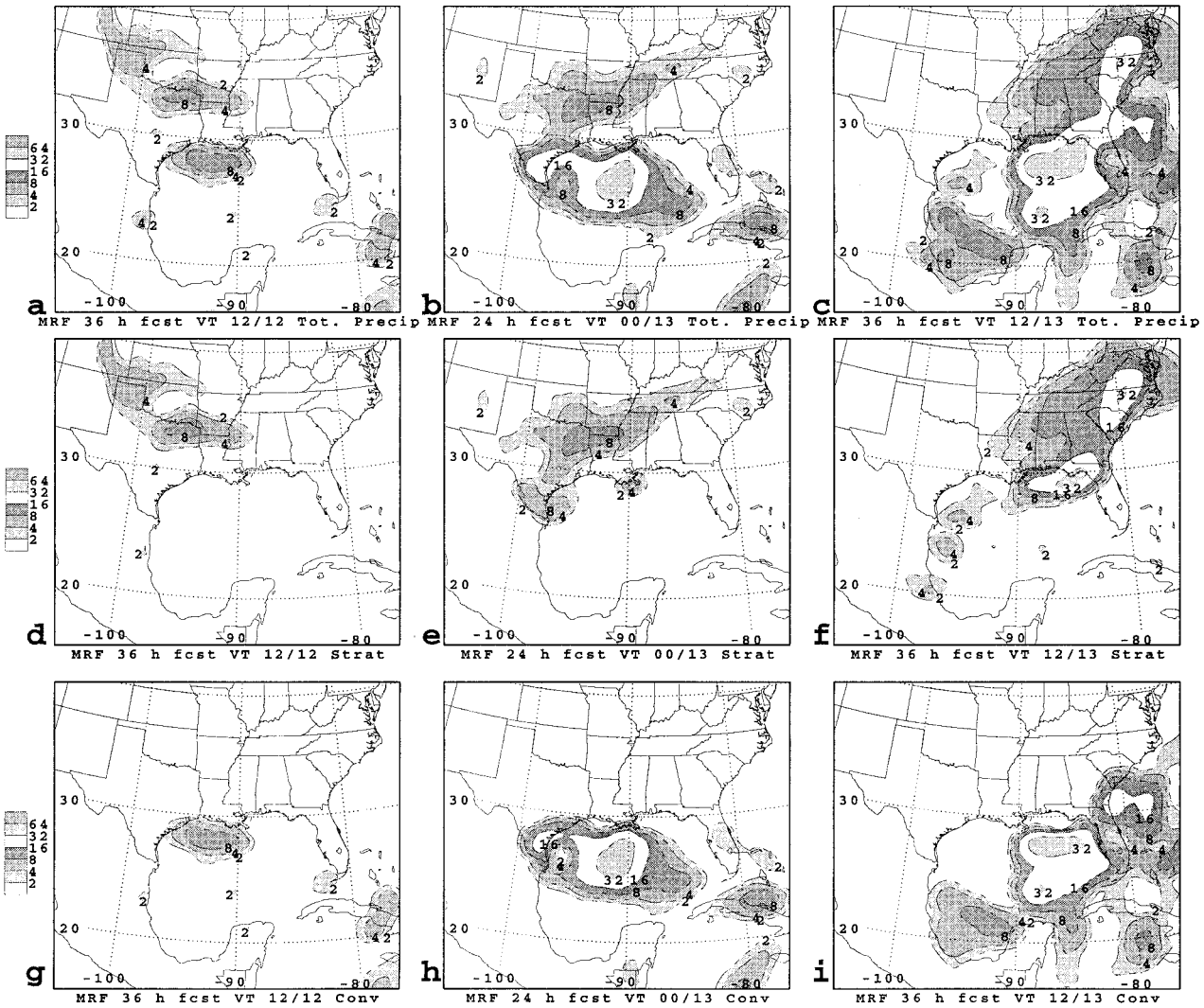

FIG. 19. Panels (a), (b), and (c) show MRF forecasts of 12 h accumulated total precipitation (mm) from the (a) 24–36-h forecast verifying 1200 UTC 12 March 1993, (b) 12–24-h forecast verifying 0000 UTC 13 March 1993, and (c) 24–36-h forecast verifying 0000 UTC 13 March 1993. Panels (d), (e), and (f) as in (a), (b), and (c) except for the stratiform contribution (mm). Panels (g), (h), and (i) as in (a), (b), and (c) except for the convective contribution (mm). Precipitation scale is shown (shaded) at left.

model to replicate the observed widespread convective outbreak in the storm environment triggered by the approach of PV anomaly C (cf. Figs. 3–8 and 19). We have discounted the possibility that the MRF representation of PV anomaly C was erroneous prior to 12/12 because the sounding data (Figs. 11a,b) disclosed that the temperature and wind fields in the vicinity of PV anomaly C were adequately initialized at 00/12. Additional indirect evidence that the representation of convection was inadequate in the MRF comes from a limited comparison of the ECMWF model forecast precipitation, height, wind, and vorticity fields (Figs. 20–22) with the MRF counterparts. Attributes of the ECMWF model forecasts relative to the MRF include a better forecast of storm track and intensity over the Gulf of Mexico (Fig. 2b), an earlier and enhanced convective precipitation over Texas and the northwestern Gulf of Mexico (cf. Figs. 19 and 20), the generation of stronger cross-contour flow toward lower heights, a more vigorous outflow jet at 250 hPa immediately downshear of the region of widespread convective heating subsequent to 12/12 (Fig. 21), and the development of substantial midlevel (500 hPa) cyclonic vorticity on the poleward periphery of PV anomaly C in the area of widespread forecast convection (Fig. 22).

The differences in the MRF and ECMWF model behavior suggest the need for a closer look at how convection is parameterized in both models. The MRF model as of March 1993, configured with 18 sigma levels in the vertical, employed a Kuo-type (Kuo 1965, 1974) cumulus parameterization scheme (Kanamitsu 1989; Kalnay et al. 1990; Kanamitsu et al. 1991; Caplan 1997,

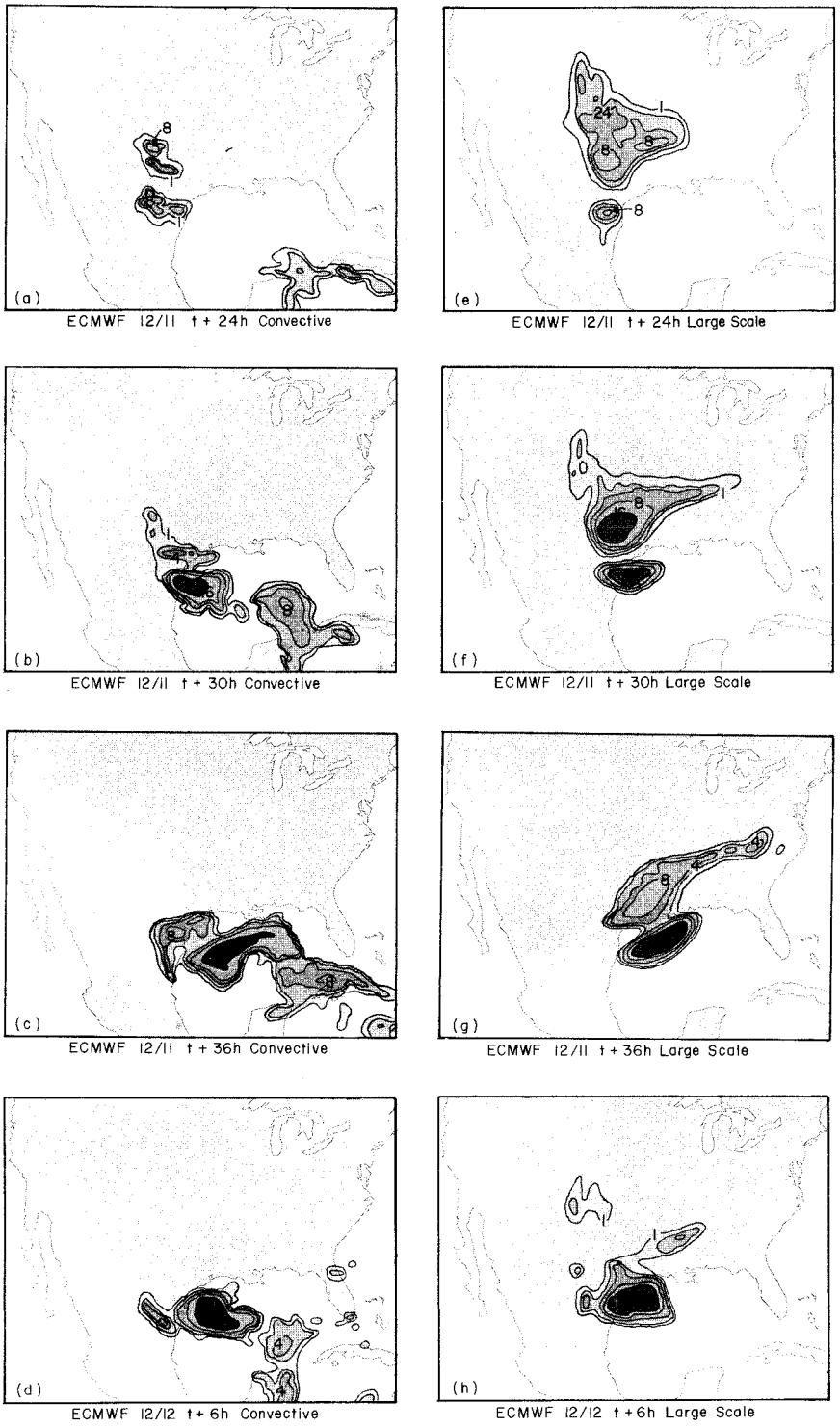

FIG. 20. ECMWF model 6-h forecast large-scale and convective precipitation forecasts as follows: convective—(a) 18–24 h verifying 12/12, (b) 24–30 h verifying 18/12, (c) 30–36 h verifying 00/13, (d) 0–6 h verifying 18/12; and large scale—(e)–(h) as in (a)–(d). Units are millimeters (shaded at intervals of 2, 4, 8, 16, 32, 64 mm as in Fig. 19).

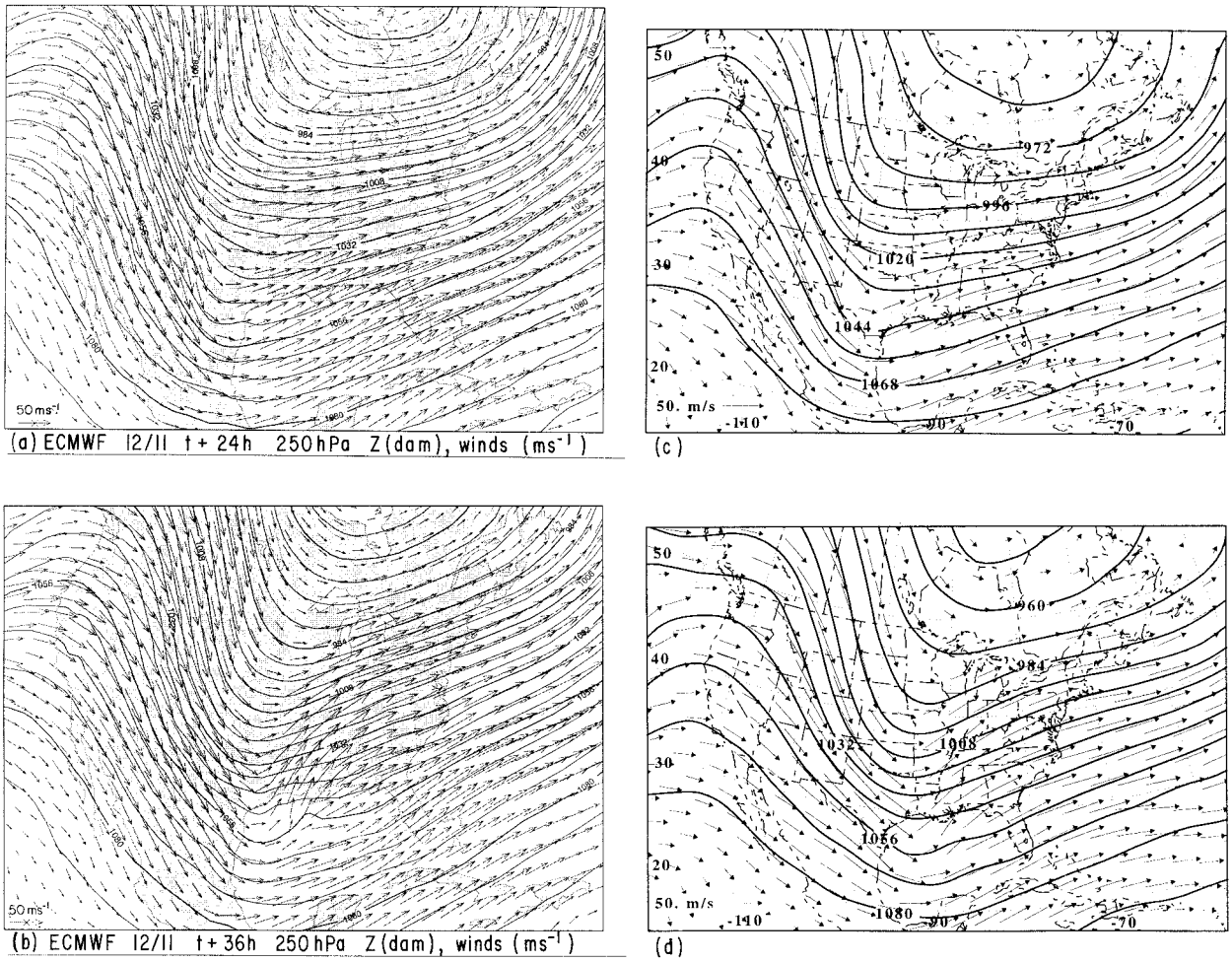

FIG. 21. ECMWF model 24 and 36 h 250-hPa height and wind forecasts verifying (a) 12/12 and (b) 00/13. Heights (solid) every 6 dam. Winds (m s^{-1}) shown by arrows; scale in lower left; (c) and (d) as in (a) and (b) except for 12- and 24-h 250-hPa MRF forecasts.

personal communication). In this scheme, convective heating can occur provided the grid columns exhibit conditional instability in the presence of moisture convergence and ascent. The vertical heating profile is derived from the difference between the model forecast sounding and the moist adiabat derived from representative temperature and moisture conditions in the planetary boundary layer (PBL). As noted by Molinari and Dudek (1992) and many others, Kuo-type cumulus parameterization schemes have a well-documented history of producing insufficient convective precipitation, consistent with the observations in this case.

According to Caplan (1997, personal communication), the MRF saturation criterion was 100% for large-scale precipitation and convection could be triggered provided the moisture convergence rate was less than -6×10^{-8} g g^{-1} s^{-1} through a vertical column whose depth was at least 30% of the model surface pressure and conditional instability and ascent were both present. The convective scheme required that the model temperature decrease upward between the second and third sigma layers (roughly 981 and 960 hPa, respectively) and that the surface temperature be greater than 5°C (ruling out elevated-base convection of the type described by Colman 1990a,b). Conditional instability was determined from parcels lifted at the second or third sigma level.

Although a detailed model investigation is beyond the scope of this paper, we have shown that there was sufficient overlap between high-CAPE regions and areas of 700-hPa ascent in the MRF initialized fields for the 24 h ending 00/13 in the incipient storm environment (Figs. 8, 14, and 18) to suggest that model forecast convection would occur, given adequate moisture convergence. We are hampered in our ability to estimate the column moisture convergence by the comparatively coarse horizontal and vertical resolution of the MRF grids. Despite these limitations, however, the moisture convergence values were above the critical column cutoff given above from near the southern tip of Texas eastward to almost 90°W by 12/12 (not shown). Given that instability and ascent were forecast to be present

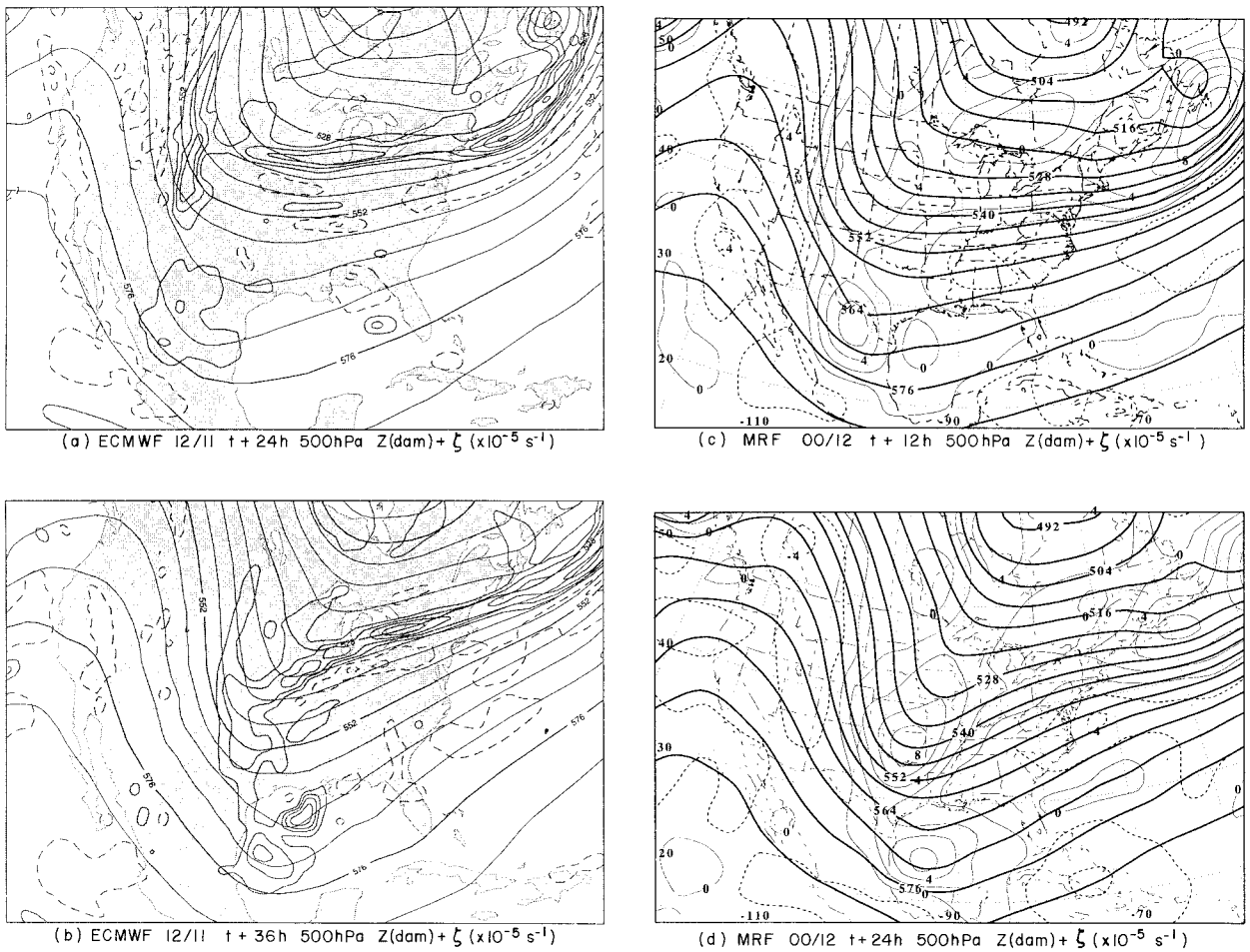

FIG. 22. As in Fig. 21 except for 500-hPa forecast heights (solid, every 6 dam) and relative vorticity. Cyclonic (anticyclonic) relative vorticity is depicted by thin solid (dashed) lines contoured every 4×10^{-5} s^{-1} (zero contour omitted) for the ECMWF model forecasts. MRF forecast vorticity is contoured every 2×10^{-5} s^{-1} (zero contour is included).

over southern Texas, the failure of the MRF to predict convective precipitation in this region may be related to an inadequate partitioning between warming and moistening in the Kuo scheme.

We know that a small area of convective precipitation for the 24–36-h period from the 00/11 MRF initialization was forecast over the northwestern Gulf of Mexico, well to the east-northeast of the observed convective region over southern Texas and the immediate coastal waters (Figs. 7d and 19g). We also know that the MRF forecast incipient cyclone track was several hundred kilometers equatorward of the area of forecast convection over the extreme northwestern Gulf of Mexico as typified by the MRF run from 00/12 shown in Fig. 2b. Although we cannot say when during any particular 12-h time period the MRF forecast convective precipitation occurred (the presence of convective precipitation in a 12-h forecast does not mean that the Kuo scheme was operative the entire time period), we can surmise with reasonable confidence that the favorable juxtaposition of deep convection near incipient cyclone centers, shown by Tracton (1973) to be important for further cyclone intensification, was not present in the MRF forecasts prior to 12/12.

The details of the ECMWF model convective scheme can be found in Tiedtke (1989). Briefly, the ECMWF model differentiates between shallow, midlevel, and deep convection. Moisture convergence is computed at each point for each model time step. It represents essentially the sum of the large-scale moisture convergence into the grid column plus moisture added by surface evaporation. Unlike the Kuo (1974) scheme there is no specific moisture convergence parameter. Instead, a cloud model determines how the converged moisture is redistributed in the column. However, when a deep layer of conditional instability and large-scale moisture convergence is present, the ECMWF essentially replicates the Kuo scheme with the important distinction that the fraction of the moisture supply that warms versus moistens the column is determined by the aforementioned cloud model instead of from the specified mois-

ture parameters as is done in the MRF version of the Kuo (1974) scheme.

We suggest that much of the advantage of the ECMWF model over the MRF in terms of forecasting the incipient SS93 cyclogenesis discussed in the opening paragraph of this section can be attributed to differences in the model cumulus parameterization schemes. In the SS93 case, the MRF 12-h and 24-h forecasts verifying 00/13 and the 12-h MRF forecast verifying 12/12 all failed to produce observed ascent and increase in θ_T over the southeastern United States and associated substantial poleward displacement of the $\theta_T = 320$–340 K contours and $p_T = 200$ hPa contour across the Tennessee and Ohio Valleys evident on the initialized DT maps for 00/13 (cf. Figs. 15 and 17). This failure resulted in a weaker thermal gradient on the DT, an associated less steeply inclined DT across the thermal gradient, and a correspondingly weaker southwesterly outflow jet ahead of the southeastward moving northern PV anomaly A. Instead, the changes in the configuration of p_T and θ_T in the MRF forecast sequence appear to be explainable in terms of quasi-adiabatic advective processes on isentropic surfaces, indicative of a relatively small impact on upper-tropospheric structure by latent heat release associated with deep convection in the model.

c. Model forecasts: Medium range

It is also of interest that the 12-h and 24-h MRF simulations discussed above produced excellent representations of PV anomaly A as it advanced southeastward toward the Gulf of Mexico by 00/13 and began to interact with PV anomaly C (Bosart et al. 1996). PV anomaly A, embedded in the northern branch of the westerlies in the amplifying confluent planetary-scale PNA flow pattern downstream of the Rockies, was associated with a relatively low DT (~400–500 hPa), modest initial surface cyclogenesis, the equatorward transport of arctic air, and also initially, an area of spotty, light stratiform precipitation. The highly baroclinic northern disturbance was ultimately responsible for the continuing spectacular development of SS93 (~960-hPa central pressure) as the storm center emerged from the Gulf of Mexico and moved northeastward toward New England. That the MRF developed a comparably deep cyclone in about the right place four days in advance (Caplan 1995; Kocin et al. 1995; Uccellini et al. 1995) following a relatively poor simulation of the initial storm development in the Gulf of Mexico suggests that the robust dynamical forcing associated with the highly baroclinic northern PV anomaly A in the amplifying confluent large-scale flow pattern would have been sufficient to produce major eastern North American cyclogenesis by itself in the presence of the natural baroclinic zone that characteristically stretches from the Gulf coast to the Atlantic coast in winter. Evidence for this speculation should be obtained from static and prognostic PV inversion techniques discussed and applied to real data cases by, for example, Davis and Emanuel (1991), Davis (1992a, b), Davis et al. (1996), and Hakim et al. (1996).

d. Perspective

Our DT analyses for the incipient stages of SS93 broadly resemble similar maps presented by Bosart and Lackmann (1995) in their analysis of the reintensification of a tropical storm (David, September 1979) over eastern North America. In the David case, the uplifting of the DT (and the associated θ_T increase) occurred over and downstream (downshear) of the storm. Massive latent heat release was occurring near and in advance of David in association with a combination of convective and stratiform precipitation. The dynamical significance of the uplifting of the DT and associated ridging downstream of David was that a favorable environment was created for surface cyclogenesis in the form of positive PV advection in the vicinity of the storm center as an otherwise weak PV anomaly approached from the west. What matters dynamically for development is the sense and strength of the positive PV advection over the cyclone center (areas of positive PV advection can be correlated with regions of observed height falls to first approximation using quasigeostrophic principles) and, in this regard, upper-tropospheric downstream ridging can be just as effective as upstream troughing in creating positive PV advection over a low-level cyclonic circulation center. This interpretation of development in terms of PV thinking (Hoskins et al. 1985) and a DT viewpoint is entirely consistent with the self-development ideas originally discussed by Sutcliffe (1947) and Sutcliffe and Forsdyke (1950) and applied, for example, by Tracton (1973) to explosive oceanic cyclogenesis.

To help put these findings in perspective, we present in Fig. 23 cross sections of PV, potential temperature, winds, and upward vertical motion from the ECMWF uninitialized (top), MRF initialized (center), and 24-h MRF forecast fields valid 00/13 (bottom). The cross-sectional lines are oriented approximately northeast-southwest and cut through the center of the rapidly strengthening low-level circulation center over the Gulf of Mexico south of Mobile, Alabama (MOB). Although the 24-h MRF forecast storm center lies somewhat to the southeast of the plane of the cross section, a few general remarks can be made. First, the DT is much more steeply inclined in the ECMWF and MRF initializations as compared to the 24-h MRF simulation on the basis of the mapped PV structure (cf. Figs. 23a–c). The DT varies from near 400 hPa (150 hPa) to the southwest (immediate northeast) of the ascent center ($< -11.0 \times 10^{-3}$ hPa s^{-1}), a variation of 250 hPa over approximately 100 km. The slope of the 1.5-PVU surface is much steeper in the ECMWF initialization (Fig. 23a). Second, whereas the potential temperature surfaces in the troposphere incline downward to the southwest in the 24-h MRF simulation there is a relative

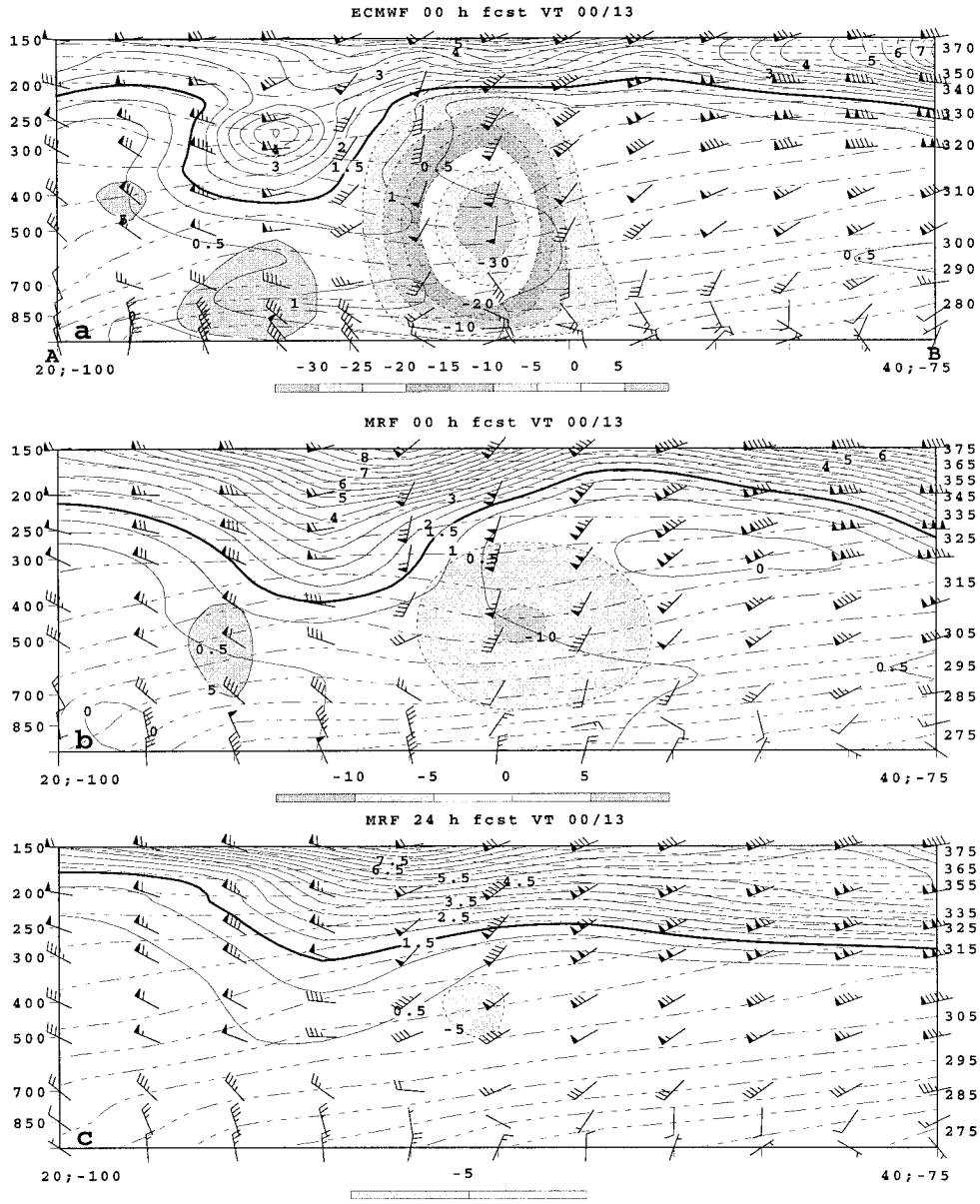

FIG. 23. Cross section from 20°N, 100°W, to 40°N, 75°W of PV (solid, every 0.5 PVU, with 1.5-PVU contour enhanced) potential temperature (thin dashed, every 5 K), wind barbs (m s^{-1}), and vertical velocity (shaded, every 5 hPa s^{-1}) for (a) ECMWF uninitialized analysis, (b) MRF initialized analysis, and (c) MRF 24-h forecast, all verifying 0000 UTC 13 March 1993. See Fig. 3 for PVU and wind speed conventions and Fig. 15 for the cross-sectional orientation.

maximum of potential temperature in the 600–300-hPa layer that closely coincides with the midtropospheric ascent maximum in the MRF initialization and the region of strong condensational heating. This initialized configuration of potential temperature and vertical motion closely matches the thermodynamic pattern expected in a region of appreciable latent heat release and associated diabatic warming as noted by Raymond and Jiang (1990) and Raymond (1992).

Our results suggest that the exceptional intensity of the incipient SS93 cyclogenesis over the Gulf of Mexico can be associated with 1) an evolving large-scale flow pattern that favored the establishment of the positive phase of the PNA pattern over North America with a deepening trough downstream of the Rockies; 2) the presence of a strong PV anomaly in the STJ that triggered the onset of widespread deep convection over southeastern Texas and offshore as it moved eastward across Mexico; 3) a positive feedback process between ascent, low-level convergence, cyclonic vorticity production, deep convection and the advection of lower values of θ_T and higher values of p_T in the presence of

a stronger than forecast low-level baroclinic zone and a stronger than analyzed SST gradient; and 4) an increase of θ_T and an associated decrease of p_T, both attributable to latent heat release downshear of the developing cyclone, that facilitated self-development through enhanced downshear ridging and the development of a strong outflow aloft.

We conclude by suggesting a need for further numerical experimentation on the role that low-level baroclinicity, surface sensible and latent heat fluxes, and convection played in the incipient SS93 development. We appreciate that these effects are highly case and model dependent as has been noted by many investigators (e.g., Bosart et al. 1995). More generally, the relationship between convection, low-level baroclinicity, and surface sensible and latent heat fluxes accompanying cyclogenesis in the presence of a strong jet stream containing embedded PV anomalies for historically difficult-to-forecast storms such as the Presidents' Day storm (Bosart 1981; Bosart and Lin; Uccellini et al. 1984, 1985, 1987; Whitaker et al. 1988) and the *QE II* storm (Gyakum 1983a,b; Uccellini 1986; Gyakum 1991; Kuo et al. 1991) might perhaps be reexamined in light of the operational model forecast problems associated with the incipient SS93 development.

Acknowledgments. This research began as part of a graduate synoptic laboratory course during the Fall 1993 semester. We wish to thank Professor John Horel at the University of Utah for making the SS93 MRF forecast grids available to the community in real time, Adrian Simmons of the European Centre for Medium-Range Weather Forecasts (ECMWF) for providing us with comprehensive SS93 plots and documentation of ECMWF model performance, and Peter Caplan of the National Centers for Environmental Prediction for helping us understand the Kuo cumulus parameterization scheme as used in the MRF at the time of SS93. We also appreciate the constructive comments of an anonymous reviewer and Mike Wallace that resulted in an improved manuscript. We thank Jeff Freedman and Paul Moore for their assistance in accessing the lightning data. We also thank Mike Cempa for his assistance in compositing the CD data. Marilyn Peacock provided drafting help and Celeste Iovinella prepared the final manuscript. This research was supported by NSF Grant ATM-9413012. Figure 8 is courtesy of Robert Bauer of the National Snow and Ice Data Center/Defense Meteorological Satellite Program.

REFERENCES

Alfonso, A. P., and L. R. Naranjo, 1996: Genesis and evolution of a severe squall over western Cuba. A case study of March 1993. *Wea. Forecasting,* **11,** 89–102.

Bosart, L. F., 1981: The Presidents' Day snowstorm of 18–19 February 1979: A subsynoptic scale event. *Mon. Wea. Rev.,* **109,** 1542–1566.

——, 1997: Observed cyclone life cycles. *The Life Cycles of Extratropical Cyclones,* M. A. Shapiro and S. Grønàs, Eds., Amer. Meteor. Soc., in press.

——, and S. C. Lin, 1984: A diagnostic analysis of the Presidents' Day snowstorm of February 1979. *Mon. Wea. Rev.,* **112,** 2148–2177.

——, and J. W. Nielsen, 1993: Radiosonde penetration of an undilute cumulonimbus anvil. *Mon. Wea. Rev.,* **121,** 1688–1702.

——, and G. M. Lackmann, 1995: Postlandfall tropical cyclone reintensification in a weakly baroclinic environment: A case study of Hurricane David (September 1979). *Mon. Wea. Rev.,* **123,** 3268–3291.

——, C. Lai, and E. Rogers, 1995: Incipient explosive marine cyclogenesis: Coastal development. *Tellus,* **47A,** 1–29.

——, G. J. Hakim, K. R. Tyle, M. A. Bedrick, M. J. Dickinson, and D. M. Schultz, 1996: Large-scale antecedent conditions associated with the 12–14 March 1993 cyclone (''Superstorm '93'') over eastern North America. *Mon. Wea. Rev.,* **124,** 1865–1891.

Boyle, J. S., and L. F. Bosart, 1986: Cyclone–anticyclone couplets over North America. Part II: Analysis of a major cyclone event over the eastern United States. *Mon. Wea. Rev.,* **114,** 2432–2465.

Burrows, W. R., R. A. Triedl, and R. G. Lawford, 1979: The southern Ontario blizzard of January 26 and 27, 1978. *Atmos.–Ocean* **17,** 306–320.

Caplan, P. M., 1995: The 12–14 March 1993 superstorm: Performance of NCEP global medium range model. *Bull. Amer. Meteor. Soc.,* **76,** 201–212.

Carr, F. H., and P. C. Kennedy, 1982: An analysis of explosive cyclogenesis over the eastern United States. Preprints, *Ninth Conf. on Weather Analysis and Forecasting,* Seattle, WA, American Meteorological Society, 285–288.

Clark, J. D., 1983: The GOES user's guide. United States Department of Commerce, Washington, DC, 7-38–7-39.

Colman, B. R., 1990a: Thunderstorms above frontal surfaces in environments without positive CAPE. Part I: A climatology. *Mon. Wea. Rev.,* **118,** 1103–1121.

——, 1990b: Thunderstorms above frontal surfaces in environments without positive CAPE. Part II: Organization and instability mechanisms. *Mon. Wea. Rev.,* **118,** 1123–1144.

Davis, C. A., 1992a: Piecewise potential vorticity inversion. *J. Atmos. Sci.,* **49,** 497–509.

——, 1992b: A potential-vorticity diagnosis of the importance of initial structure and condensational heating in observed extratropical cyclogenesis. *Mon. Wea. Rev.,* **120,** 2409–2428.

——, and K. A. Emanuel, 1991: Potential vorticity diagnostics of cyclogenesis. *Mon. Wea. Rev.,* **119,** 2309–2330.

——, E. D. Grell, and M. A. Shapiro, 1996: The balanced dynamical nature of a rapidly intensifying oceanic cyclone. *Mon. Wea. Rev.,* **124,** 3–26.

DeAngelis, R. M., and Coauthors, 1993: Was it the storm-of-the-century? *Mar. Wea. Log,* **37,** 38–45.

Gilhousen, D. B., 1994: The value of the NDBC observations during March 1993's ''storm of the century.'' *Wea. Forecasting.* **9,** 255–264.

Grumm, R. H., and J. R. Gyakum, 1986: Systematic surface anticyclone errors in NMCs limited-area fine mesh and spectral models during the winter of 1981/82. *Mon. Wea. Rev.,* **114,** 2329–2343.

Gyakum, J. R., 1983a: On the evolution of the QE II storm. I: Synoptic aspects. *Mon. Wea. Rev.,* **111,** 1137–1155.

——, 1983b: On the evolution of the QE II storm. II: Dynamic and thermodynamic structure. *Mon. Wea. Rev.,* **111,** 1156–1173.

——, 1991: Meteorological precursors to the explosive intensification of the *QE II* storm. *Mon. Wea. Rev.,* **119,** 1105–1131.

——, and E. S. Barker, 1988: A case study of explosive sub-synoptic scale cyclogenesis. *Mon. Wea. Rev.,* **116,** 2225–2253.

——, Y.-H. Kuo, Z. Guo, and Y.-R. Guo, 1995: A case of rapid continental mesoscale cyclogenesis. Part II: Model and observational diagnosis. *Mon. Wea. Rev.,* **123,** 998–1024.

Hakim, G. J., L. F. Bosart, and D. Keyser, 1995: The Ohio Valley

wave merger cyclogenesis event of 25–26 January 1978. Part I: Multiscale case study. *Mon. Wea. Rev.,* **123,** 2263–2992.
——, D. Keyser, and L. F. Bosart, 1996: The Ohio Valley wave merger eyclogenesis event of 25–26 January 1978. Part II: Diagnosis using quasigeostrophic potential vorticity inversion. *Mon. Wea. Rev.,* **124,** 2176–2205.
Hoskins, B. J., 1990: Theory of extratropical cyclones. *Extratropical Cyclones*: *The Erik Palmen Memorial Volume,* C. W. Newton and E. O. Holopainen, Eds., Amer. Meteor. Soc., 63–80.
——, and P. Berrisford, 1988: A potential vorticity perspective of the storm of 15–16 October 1987. *Weather,* **23,** 122–129.
——, M. E. McIntyre, and A. W. Robertson, 1985: On the use and significance of isentropic potential vorticity maps. *Quart. J. Roy. Meteor. Soc.,* **111,** 877–946.
Hsu, S. A., 1993: The Gulf of Mexico—A breeding ground for winter storms. *Mar. Wea. Log,* **37,** 4–11.
Huo, Z., D.-L. Zhang, J. R. Gyakum, and A. Stantiforth, 1995: A diagnostic analysis of the superstorm of March 1993. *Mon. Wea Rev.,* **123,** 1740–1761.
Kalnay, E., M. Kanamitsu, and W. E. Naker, 1990: Global numerical weather prediction at the National Meteorological Center. *Bull. Amer. Meteor. Soc.,* **71,** 1410–1428.
Kanamitsu, M., 1989: Description of the NMC Global Data Assimilation and Forecast System. *Wea. Forecasting,* **4,** 335–342.
——, and Coauthors, 1991: Recent changes implemented into the Global Forecast System at NMC. *Wea. Forecasting,* **6,** 425–435.
Koch, S. E., M. Desjardins, and P. J. Kocin, 1983: An interactive Barnes Scheme for use with satellite and conventional data. *J. Climate Appl. Meteor.,* **22,** 1487–1503.
Kocin, P. J., P. N. Schumacher, R. F. Morales, and L. W. Uccellini, 1995: Overview of the 12–14 March 1993 superstorm. *Bull. Amer. Meteor. Soc.,* **76,** 165–182.
Kuo, H. L., 1965: On the formation and intensification of tropical cyclones through latent heat release by cumulus convection. *J. Atmos. Sci.,* **22,** 40–63.
——, 1974: Further studies of the parameterization of the influence of cumulus convection on large-scale flow. *J. Atmos. Sci,* **31,** 1232–1240.
Kuo, Y.-H., M. A. Shapiro, and E. G. Donall, 1991: The interaction between baroclinic and diabatic processes in a numerical simulation of a rapidly intensifying extratropical marine cyclone. *Mon. Wea. Rev.,* **119,** 368–384.
——, J. R. Gyakum, and Z. Guo, 1995: A case of rapid continental mesoscale cyclogenesis. Part I: Model sensitivity experiments. *Mon. Wea. Rev.,* **123,** 970–997.
Lackmann, G. M., D. Keyser, and L. F. Bosart, 1997: A characteristic life cycle of upper-tropospheric cyclogenetic precursors during the Experiment on Rapidly Intensifying Cyclones over the Atlantic (ERICA). *Mon. Wea. Rev.,* **125,** 2729–2758.
Mass, C. F., H. J. Edmon, H. J. Friedman, N. R. Cheney, and E. E. Recker, 1987: The use of compact discs for the storage of large meteorological and oceanographic data sets. *Bull. Amer. Meteor. Soc.,* **68,** 1556–1558.
McIntyre, M., 1988: The dynamical significance of isentropic distributions of potential vorticity and low-level distributions of potential temperature. *Proc. Nature and Prediction of Extratropical Weather Systems,* Vol. 1, Reading, United Kingdom, European Centre for Medium-Range Weather Forecasts, 237–259.
Mesinger, F., 1996: Forecasting cold surges east of the Rocky mountains. Preprints, *15th Conf. on Weather Analysis and Forecasting,* Norfolk, VA, Amer. Meteor. Soc., 68–69.
Molinari, J., and M. Dudek, 1992: Parameterization of convective precipitation in mesoscale numerical models: A critical review. *Mon. Wea. Rev.,* **120,** 325–344.
Orlanski, I., and J. P. Sheldon, 1995: Stages in the energetics of baroclinic systems. *Tellus,* **47A,** 605–628.
Petterssen, S., 1955: A general survey of factors influencing development at sea level. *J. Meteor.,* **12,** 36–42.
Raymond, D. J., 1992: Nonlinear balance and potential vorticity thinking at large Rossby number. *Quart. J. Roy. Meteor. Soc.,* **118,** 987–1015.
——, and H. Jiang, 1990: A theory for long-lived mesoscale convective systems. *J. Atmos. Sci.,* **47,** 3067–3077.
Roebber, P. J., 1984: Statistical analysis and updated climatology of explosive cyclones. *Mon. Wea. Rev.,* **112,** 1577–1589.
——, 1989: The role of surface heat and moisture fluxes associated with large-scale ocean current meanders in maritime cyclogenesis. *Mon. Wea. Rev.,* **117,** 1676–1694.
Salmon, E. W., and P. J. Smith, 1980: A synoptic analysis of the 25–26 January 1978 blizzard cyclone in the central United States. *Bull. Amer. Meteor. Soc.,* **61,** 453–460.
Sanders, F., and J. R. Gyakum, 1980: Synoptic-dynamic climatology of the ''bomb.'' *Mon. Wea. Rev.,* **108,** 1589–1606.
Schultz, D. M., W. E. Bracken, L. F. Bosart, G. J. Hakim, M. A. Bedrick, M. J. Dickinson, and K. R. Tyle, 1997: The 1993 superstorm cold surge: Frontal structure, gap flow, and tropical impact. *Mon. Wea. Rev.,* **125,** 5–39; Corrigendum, **125,** 662.
Sutcliffe, R. C., 1947: A contribution to the problem of development. *Quart. J. Roy. Meteor. Soc.,* **73,** 370–383.
——, and A. G. Forsdyke, 1950: The theory and use of upper air thickness patterns in forecasting. *Quart. J. Roy. Meteor. Soc.,* **76,** 189–217.
Tiedtke, M., 1989: A comprehensive mass flux scheme for cumulus parameterization in large-scale models. *Mon. Wea. Rev.,* **117,** 1779–1800.
Tracton, M. S., 1973: The role of cumulus convection in the development of extratropical cyclones. *Mon. Wea. Rev.,* **101,** 573–593.
Uccellini, L. W., 1986: The possible influence of upstream upper-level baroclinic processes on the development of the QE II storm. *Mon. Wea. Rev.,* **114,** 1019–1027.
——, P. J. Kocin, R. A. Petersen, C. H. Wash, and K. F. Brill, 1984: The Presidents' Day cyclone of 18–19 February 1979: Synoptic overview and analysis of the subtropical jet streak influencing the precyclogenetic period. *Mon. Wea. Rev.,* **112,** 31–55.
——, D. Keyser, K. F. Brill, and D. H. Wash, 1985: The Presidents' Day cyclone of February 1979: Influence of upstream trough amplification and associated tropopause folding on rapid cyclogenesis. *Mon. Wea. Rev.,* **113,** 962–988.
——, R. A. Petersen, K. F. Brill, P. J. Kocin, and J. J. Tuccillo, 1987: Synergistic interactions between an upper-level jet streak and diabatic processes that influence the development of a low-level jet and a secondary coastal cyclone. *Mon. Wea. Rev.,* **115,** 2227–2261.
——, P. J. Kocin, R. S. Schneider, P. M. Stokols, and R. A. Dorr, 1995: Forecasting the 12–14 March 1993 superstorm. *Bull. Amer. Meteor. Soc.,* **76,** 183–199.
Walker, N. D., 1993: A preliminary look at cyclogenesis in Gulf of Mexico during the March 1993 blizzard. *Mar. Wea. Log,* **37** (2), 89.
Wallace, J. M., and D. S. Gutzler, 1981: Teleconnections in the geopotential height field during the Northern Hemisphere winter. *Mon. Wea. Rev.,* **109,** 784–812.
Weiss, S. J., 1992: Some aspects of forecasting severe thunderstorms during cool-season return flow episodes. *J. Appl. Meteor.,* **31,** 964–982.
Whitaker, J. S., L. W. Uccellini, and K. F. Brill, 1988: A model-based diagnostic study of the rapid development phase of the Presidents' Day cyclone. *Mon. Wea. Rev.,* **116,** 2337–2365.